Influence of Free Ferrite Content on the Machinability of GCI using CBN Tool

By

Yesong (Luke) Liu, Mechanical. Eng

(McMaster University, Canada)

A Thesis

Submitted to the School of Graduate Studies

in Partial Fulfilment of the Requirements

for the Degree

Master of Applied Science

McMaster University

MASTER OF APPLIED SCIENCE (2018) McMaster University

(Mechanical Engineering) Hamilton, Ontario

TITLE: Influence of Free Ferrite Content on the Machinability of GCI using CBN Tool

AUTHOR: YeSong Liu (McMaster University, Canada)

SUPERVISOR: Dr. Stephen C. Veldhuis

Department of Mechanical Engineering

McMaster University

NUMBER OF PAGES: x, 85

Abstract

Over the years, industrial partners experienced issues related to inconsistent free ferrite in gray cast iron. In the course of a hot summer and a cold winter, machinability balance varies up to 350%. During warm months it is better and cold months worse. The inconsistent machinability increases the scrap rates by up to 400% and reduces tool life by up to 70%. The ultimate objective of this research is to collaborate with an automotive industrial partner to investigate the periodic machinability variability of gray cast iron engine sleeves, with a goal to reduce the cost and scrap rate of tool inserts. In this study, a significant amount of work was conducted concerning sample preparation for a metallography check. Samples from different months with varying amount of "free ferrite" were collected to study the seasonal effect on their machinability and high-speed machining under similar industrial conditions. Furthermore, a room temperature age strengthening of gray cast iron was conducted to demonstrate how the hardness increase from aging could improve the machinability of gray cast iron.

A CBN insert is the second hardest cutting tool after the diamond insert, and is widely used in industry for machining cast iron. It has a high cutting speed is commonly used due to its high hardness and impressive wear resistance. It is known that gray cast iron can naturally age at room temperature or artificially age under a controlled temperature. Under different aging temperatures and times, gray cast iron exhibits a greater hardness after age strengthening, which affects the CBN tool life. The latter is usually limited by flank wear length, however the content of free ferrite in gray cast iron can generate ferrous built-up on the CBN cutting edge and significantly shorten the tool life of the CBN cutting tool.

Acknowledgements

First, and the most important, I would like to thank my supervisor, Dr. Stephen C. Veldhuis. He is my mentor and all of his research guidance supported me during my study at MMRI. He is patient, kindly and encouraging to myself and all MMRI colleagues in their life and studies. I would also like to thank all the other amazing and helpful colleagues at team MMRI.

I'm grateful to the technicians from Material Engineering department, Xiaogang Li and Doug Culley. Their help with operating all of the equipment supported me in finishing my research.

I would like to thank Dr. Abul Fazal M. Arif for his detailed and patient guidance with my entire research organization and thesis writing. Also, great thanks to Simon Oomen-Hurst for the rich opportunity he provided to me in working on an industrial project with him. The excellent work experience gained from those projects, benefited my problem-solving skills.

I would like to acknowledge Ahmed Sweed, Baoqin Deng and Bipasha Bose for their training and technical support throughout my work.

I would like to acknowledge CANRIMT for their financial contributions.

Lastly, I would like to thank my wife. Her endless love and support throughout my research as well as daily life, aided me in finishing my study. Without her it wouldn't have been possible for me.

Table of Content

List of Figures

List of Tables

Chapter 1: Introduction

This topic is based on the study of metallography and machining of GCI. Metallography is nothing but the selection of the best metallurgical tools for investigating the property of certain materials [1] and machining is a metal removal process for altering the bulk material into a desired shape. This is achieved by removing small layers of the workpiece material into chips with an edge prepared tool. Recipes of polishing and etching solutions are described later for the study of the microscope images which were polished to 1µm level of surface roughness. The automotive partner manufactures GCI sleeves through a high-speed turning process to achieve a specific high production rate and efficiency. It was proven that CBN tools are capable of high-speed machining with a high production efficiency [2], [3]. Therefore, the machining operation is to basically mimick the cutting conditions (cutting speed, feed rate, depth of cut) and the industrial partner is to make sure that the results are authentic and representative of actual practice.

1.1. Gray Cast Iron

The history of using GCI can be traced back thousands of years. In modern times, GCI is the most widely used cast iron in industrial applications, since it has good tool wear resistance, low power requirement and high machinability. Its favorable damping capacity and good surface finish [4]makes GCI one of the best materials for engine sleeves. The name “gray” cast iron originates from its fracture surface which is the color of graphite flakes [5]. Pre-existing cracks help generate discontinuous chips which are easily removed [6]. GCI can be machined with conventional carbide cutting tools at relatively low cutting speeds of around 300m/s or cut with cubic Boron Nitride (CBN) inserts under a high-speed machining process with speeds up to 1000m/s.

To satisfy the market demand at the same time as maintaining a high production efficiency with relatively low production cost, most industrial companies would like to increase the cutting speed while keeping the tool life at a reasonable range.

Traditional carbide tools or ceramic tools are no longer suitable for high speed machining; under severe cutting conditions, practical use has demonstrated that CBN cutting tools can cut cast iron or hardened steel with promising tool life and high efficiency [3]. Although, CBN is best option for cutting GCI at high speeds, the content of free ferrite has to be limited. Traceable amount of free ferrite can cause significant CBN tool wear, therefore in this study, the free ferrite content of workpiece materials was chosen to be from 1% to around 10%.

1.2. Phenomenon of Age Strengthening

Certain gray cast iron grades experience a very interesting, but little understood phenomenon. After casting and cooling to room temperature, a gray cast iron part left undisturbed at room temperature in open air will undergo microstructural changes. In general, the aging process progresses in a non-linear fashion, with major changes occurring quickly in the first 5 - 7 days after casting, and more gradual changes continuing for up to 60 days after casting. The aging process can increase the tensile strength of the cast iron by up to 15% but can increase machinability by up to 500%. This represents a fantastic opportunity for industry to understand the optimal machining age of GCI or other cast iron products for maximization of productivity and tool life.

The aging phenomenon was first identified in 1955 [7], but little research has been conducted on understanding this phenomenon, until the 1990's when researchers Nicola and Richards rekindled this subject [8]. Since then, several studies were completed to understand this phenomenon, but these have been limited to a few specific grades of gray cast iron. The research to date provides a solid foundation for investigating the aging process, and predicts the aging progress in GCI engine sleeves.

1.3. Seasonal Effect

Over the course of several months, the variation of product machinability is common in industry; typically, due to the uncontrolled temperature of the atmosphere causing the variation in the cooling rates of casting material during hot and cold months. As shown in Figure 1.3-1, the industrial partner has issues based on seasonal ambient temperature; the machinability of their product was relatively poor in cold months and relatively good in warm months between 2013 to 2015. In addition to seasonal issues, gray cast iron engine sleeves are known to age strengthen at an ambient temperature over the course of 10 – 30 days. An inconsistent ambient temperature could affect the aging rate and create the variable machinability over this period.

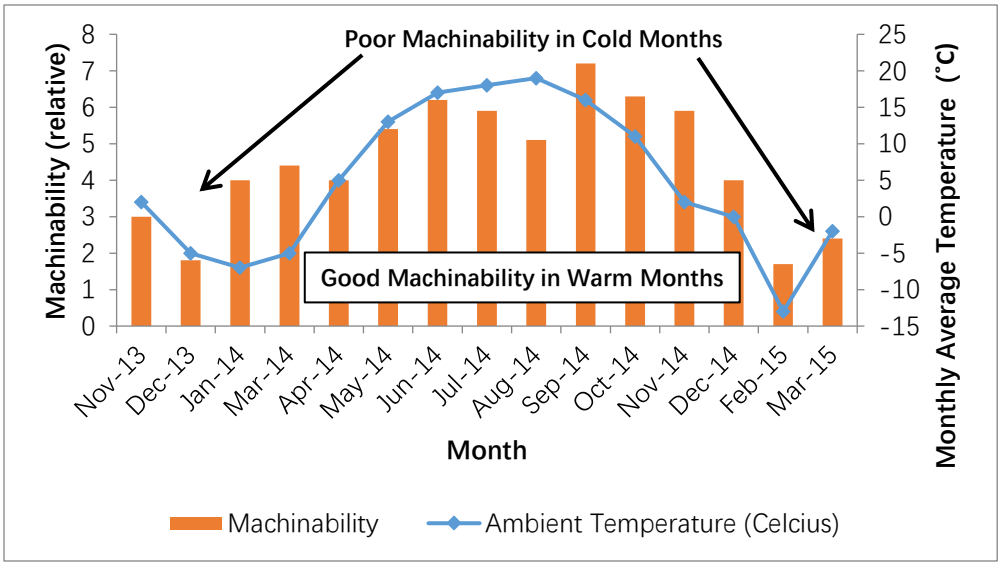

Figure 1.3-1 Machinability changes with months.

1.4. Objectives and Motivation

1.4.1. Objectives

The primary objective of this work is to study varying machinability of GCI cutting under High Speed Machining with a CBN cutting tool. This objective is broken down into the following specific aims:

- To optimize the best fitting CBN cutting tool as well as the cutting conditions for all of the following studies.

- To observe how the content of free ferrite in GCI engine sleeves affect the machinability of a CBN cutting tool under an industrial high-speed turning process.

- To mimick the room temperature aging process that the industrial partner conducted to demonstrate how the age strengthening process can improve the machinability of GCI and the impact of its free ferrite content.

  To demonstrate that the seasonal effect in industry is majorly affected by the content of free ferrite.

1.4.2. Motivation

The industrial partner in Ontario manufactures thousands of engine blocks per day which include grey cast iron cylinder sleeves. By eliminating factors that affect the machinability of GCI, significant savings on tool life and scrap costs can be achieved, and the additional benefits to production and personnel are difficult to estimate. Overall, improving GCI engine sleeve machining can be of interest to many automotive companies.

1.5. Methodology

Samples were collected from different warm and cold months for microscopical study. The elemental content, graphite types and their matrix composition were compared using polished microscopic images and EDS mapping. Likewise, Vicker's hardness results collected from each sample were used to analyze whether there was any micro-hardness difference between samples from warm and cold months. Later on, fresh/unaged samples with a range of 1 – 10% of "free ferrite" were chosen for the high-speed turning test. CBN inserts were selected to test the influence of age strengthening on machinability as well as the extent "free ferrite" negatively affects CBN tool life.

1.6. Thesis Outline

Chapter 1 of this thesis explains the major objectives and the motivation of this research study. Literature review about workpiece material and theories are covered in chapter 2. All the experimental setup and procedures are detailly described in chapter 3. Chapter 4 and chapter 5 are preliminary tests, which provides the optimal choice of CBN cutting insert and cutting speed. The results and discussions about influence of free ferrite content on machinability of gray cast iron are provided in chapter 6. The results about gray cast iron age strengthening and its influence on machinability are illustrated in chapter 7. Chapter 8 illustrates the reason of seasonal change of gray cast iron machinability. Eventually, conclusions and future research suggestions are provided in chapter 9.

Chapter 2: Literature Review

2.1. Cast Iron

Similar to the steel family, the term cast iron refers to a large family of ferrous alloys which amounts to more than 70% of total world's production tonnage [9]. Cast iron are primarily iron alloys with major carbon (>2%) and silicon content (>1%). Since cast iron has a higher carbon content than steel, the structure of cast iron exhibits a rich carbon phase [10].

Cast irons are multicomponent ferrous alloys, which solidify with a eutectic. Thermodynamically metastable Fe-Fe3C system and the stable Fe-Gr system can be achieved by balancing the content of C and Si, by the composition of alloying elements, and by control of founding, cooling, and heat-treating processes. Under the metastable path, the majority of the carbon phase in the eutectic forms iron carbide is Fe3C; on the other hand, under the stable solidification path, the majority of the carbon phase is graphite. These two types of eutectics – the stable Fe-Gr (austenite – graphite) and the metastable Fe-Fe3C (austenite – iron carbide) are the most basic iron phases with significant differences in their mechanical properties. Therefore, categories of the type, amount and morphology of the eutectic are capable of achieving desired mechanical properties [11].

2.1.1. Classification – Gray Cast Iron

In History, the earliest classification of cast iron was based on its fractured surface colors, which are gray iron and white iron. Typically, as its name suggests, white iron exhibits a white crystalline fracture surface because the rich carbon phase is metastable iron carbide (Fe_3C). Gray iron has a gray fracture surface because of its rich graphite flakes and the stable solidified graphite eutectic does not reflect light. As

metallography advanced, cast iron can be classified based on the following microstructural features [11]:

- **Graphite type**: Lamellar (flake) graphite, spheroidal (nodular) graphite, compacted (vermicular) graphite, and temper graphite
- **Matrix**: Ferritic, pearlitic, austenitic, martensitic, and bainitic (austempered)

In industry, the classification can be simplified as common cast irons for general purpose applications or special cast irons for special applications. In the end, the final combination of all classification of cast iron is shown in Table 2.1, which is adapted from "Metals Handbook Desk Edition", 2nd edition edited by Joseph R. Davis in 1998 [10].

Table 2.1: Classification of cast irons by commercial designation, microstructure, and fracture (based on [10]).

Commercial designation	Graphite	Matrix[(a)]	Fracture	Final structure after
Gray cast iron	Lamellar	P	Gray	Solidification
Ductile iron	Spheroidal	F, P, A	Silver – gray	Solidification or heat treatment
Compacted graphite iron	Compacted (vermicular)	F, P	Gray	Solidification
White iron	Fe_3C	F, M	White	Solidification and heat treatment[(b)]
Mottled iron	Lamellar Gr + Fe_3C	P	Mottled	Solidification
Malleable iron	Temper	F, P	Silver – gray	Heat treatment
Austempered ductile iron	Spheroidal	At	Silver – gray	Heat treatment

(a) F, ferrite; P, pearlite; A, austenite; M, martensite; At, austempered (bainite).

(b) White irons are not usually heat treated, except for stress relief and to continue austenite transformation.

Gray cast iron (GCI) was named after its gray fracture surface and is the most commonly used cast iron all over the world in the entire industrial history. Many industrial companies use GCI for their products, for instance, automotive engine blocks and sleeves,

machine tool base, transformation pipes, enclosures, housings and an uncountable number of other products. GCI normally contains 2.5% - 4% carbon and 1% - 3% silicon. By artificially controlling the casting processes and the elemental content, the rich carbon phase forms irregular graphite precipitations and the iron matrix gets saturated with elongated and curved graphite flakes. The latter work as natural crakes and provide good damping characteristics as well as good machinability, since the flakes enhance chip breaking and lubricate the cutting tools. For many applications requiring good wear resistance, GCI is favored due to the graphite flakes. However, they also concentrate stress and result in brittleness, a property not only common to GCI but also to all cast irons [12].

2.1.2. Microstructure of GCI

The research focused on cylinder liner, aka "engine sleeve" as Figure 2.1-1 is the most important part of a vehicle engine block. The engine sleeve operates under severe conditions, long life cycles and high temperatures and pressures; meanwhile, the piston and piston rings rub against the internal surface of the sleeves, which requires the material to possess a sufficient wear resistance for long service life. Cast iron or specifically GCI are used in most cases [13].

Figure 2.1-1 Engine sleeves and engine block.

Table 2.2 presents the cross references of international equivalent standards and grades of GCI based on ISO – 185. Here in this research, the engine sleeves were made

from the FC250 grade of GCI. The ISO standard specifies the GCI grades by a combination of minimum tensile strength, which is 250 N/mm2 in all the cases shown in Table 2.2.

Table 2.2: Cross references of ISO 185 grade designations. (based on ISO 185 [14]).

Country/Field	Standard	Grade (250 N/mm^2)
UK/Europe	EN 1561	EN-GJL-300
USA	ASTM A48	250
Japan	JIS G5501	FC250
SAE[(a)]	SAE J431	G11H20
(a) SAE – surface vehicle standard [15]		

Different applications need a certain grade of GCI for special requirements. In North America, the ASTM standard is the most familiar for engineers to specify GCI by using tensile strength expressed in MPa or ksi. GCI are classified as an increase from class 150 (minimum tensile strength of 150 MPa or 20 ksi) to class 400 (minimum tensile strength of 400 MPa or 60 ksi) by ASTM classification [16]. Generally speaking, the following properties of GCI are assumed to increase alongside tensile strength to form class 150 to 400 [10]:

- Strength
- Final surface finish
- Modulus of elasticity
- Wear resistance

On the other hand, the following properties of GCI are assumed to decrease with increasing tensile strength and based on the preferred properties, the class of GCI should be chosen wisely:

- Machinability
- Thermal shock resistance
- Damping capacity
- Ability to be cast in thin sections

Matrix

For GCI, the main elements of chemical composition are carbon and silicon. The mechanical properties of GCI mainly depend on the iron matrix (pearlite matrix or ferrite matrix) and minimally influenced by the type of graphite. A relatively low cooling rate and relatively high carbon and silicon content is likely to produce a ferrite matrix (pure iron phase) which has low strength but high ductility, since the high silicon content increases the graphitization potential and the carbon dissolved in iron deposits onto the existing graphite flake structure in process of slow cooling. On the other hand, rapid cooling prevents the carbon from dissolving into the graphite flakes, which increase the hardness and tensile strength of GCI and produce a pearlite matrix (iron carbide). Minor alloying elements such as manganese, sulfur, phosphorous, aluminum, nickel, lead and many other alloying elements can significantly affect both the microstructure of the matrix and the morphology of graphite [11], [17]. The best case is the content of manganese and sulfur, both of which are common minor elements in the composition of GCI. Manganese is a strong pearlite promoter and the relatively high content of manganese helps to produce a pearlite matrix. If the content of the manganese and sulfur is well balanced, a manganese sulfide (MnS) will form, which helps to lubricate the cutting tool and improve the machinability [18], [19].

The combination of all major and minor elements of chemical composition can be summarized by the carbon equivalent (CE), which simply describes how the different content of elements influence the tensile strength of GCI. The simplest form of CE only accounts for the content of carbon and silicon as shown as equation 2.1, if all the common elements are involved, the CE is represented by equation 2.2.

$$\mathrm{CE} = \%\mathrm{C} + (1/3)(\%\mathrm{Si}) \tag{2.1}$$

$$\mathrm{CE} = \%\mathrm{C} + 0.3(\%\mathrm{Si}) + 0.33(\%\mathrm{P}) - 0.027(\%\mathrm{Mn}) + 0.4(\%\mathrm{S}) \tag{2.2}$$

Graphite

Similar to the iron matrix, the cooling rate and both major and minor elemental composition have a strong influence on the morphology of graphite flakes. Five types of graphite flakes (Type A – Type E) are classified by ISO 945 based on their graphite microstructure in GCI through comparative visual analysis. The mechanical properties of GCI are not only affected by the matrix but also by the shape, size, amount, and distribution of the graphite flakes. The five graphite flake distributions are shown as Figure 2.1-2.

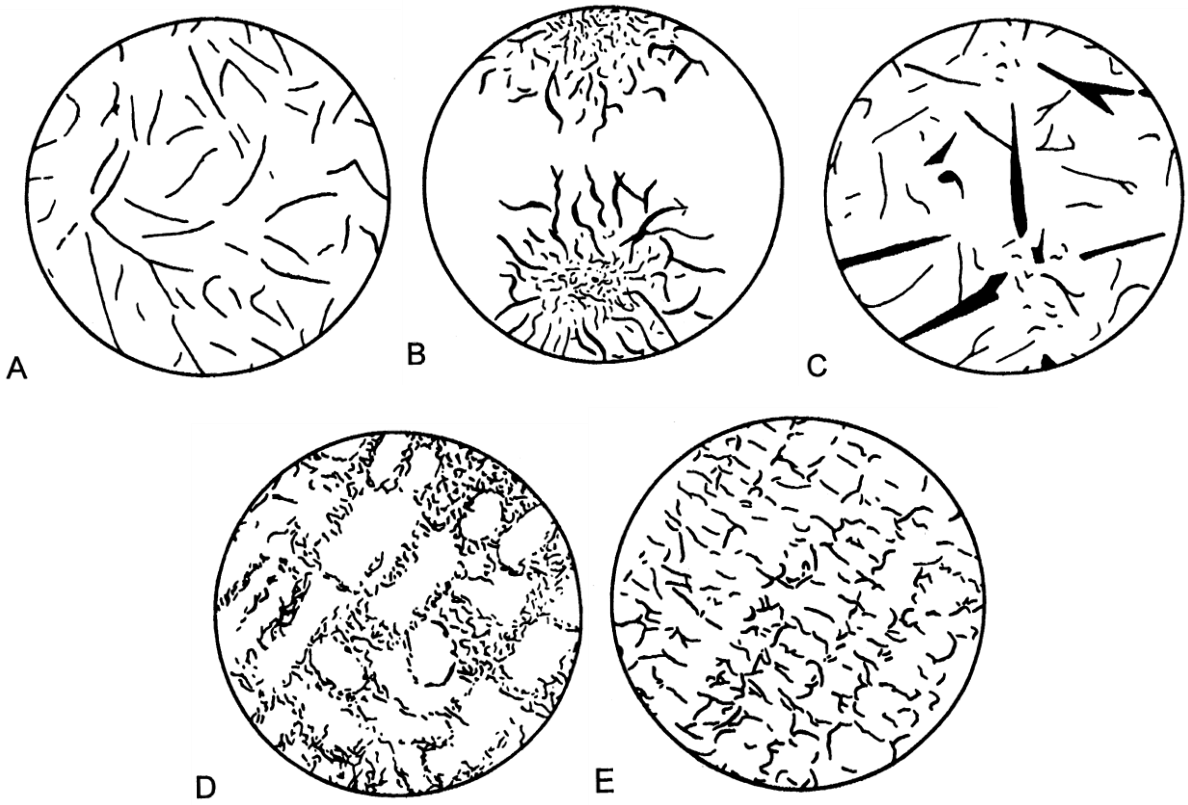

Figure 2.1-2 GCI graphite distributions. (based on ISO 945-1:2008 [20]*)*

Type A graphite flake distributes as a random orientation, and compared to all other types of graphite, it has the best mechanical properties and is favorable for most of the applications. The Type B graphite flake exhibits a rosette pattern and is formed with a greater amount of undercooling. Usually, the type B graphite flake appears on common

moderately thin sections or along the surface of thicker sections. The Type C graphite flake distinctively reduces the mechanical properties of GCI and produces rough surfaces after machining. It occurs in hypereutectic irons due to minimum undercooling. However, the type C graphite flake can be used for applications requiring a product with a high thermal conductivity and damping capacity. Both type D and type E graphite flakes form with a high amount of undercooling and without a sufficient amount of carbide formation. Type D graphite flakes have a random orientation while type E graphite flakes have a directed orientation. The following table summarizes the details of graphite distributions in GCI [10].

Table 2.3: Graphite distributions in GCI. (based on [10])

Distribution	Main 2D appearance	Occurrences
A	Apparently uniform distribution	Cast iron solidified with a low to intermediate degree of undercooling.
B	Rosette graphite with undercooling graphite	Cast iron solidified with an intermediate degree of undercooling, particularly thin-walled castings.
C	Aggregate of larger graphite flakes surrounded by smaller, randomly oriented graphite flakes (eutectic graphite)	Hypereutectic cast iron.
D	Finely branched graphite Fine, randomly oriented graphite flakes in the interdendritic position	Cast iron solidified with a high degree of undercooling. The distribution can be associated with other distributions (for example A and/or B and/or E).
E	Preferentially orientated graphite flakes in the interdendritic position	Cast iron with low carbon equivalent, solidified with low or moderate undercooling. Local area corresponding to a plane of polish cutting through the main axis of some highly oriented dendrites.

Overall, not only do the types of graphite influence mechanical properties but also the size of graphite flakes. A slow cooling rate and high CE values produce large graphite flakes. GCI with large flakes have a week tensile strength but better thermal conductivity and damping capacity. On the other hand, small graphite flakes are formed

under rapid solidification and provide a better tensile strength and a fine, smooth surface finish.

2.1.3. GCI Chemical Composition

A typical unalloyed common GCI is formed with iron, followed by 2.5 – 4% of carbon and 1.0 – 3.0% of silicon, similar to the composition of Manganese (0.2 – 1.0%), Phosphorus (0.002 – 1.0%) and Sulphur (0.02 – 0.25%) [5], [11]. A list of alloying elements can contribute to the common GCI to enhance the mechanical properties by influencing both the graphitization potential and the microstructure of GCI. Elements that have a high positive graphitization potential are listed below in order of decreasing positive potential from top to bottom:

- Carbon
- Tin
- Phosphorus
- Silicon
- Aluminum
- Copper
- Nickel

Visa versa, elements that have high negative graphitization potential are listed below in order of increasing negative potential from top to bottom:

- Manganese
- Chromium
- Molybdenum
- Vanadium
- Tungsten

The ranges of typical alloying elemental content are shown in the following table:

Table 2.4: Ranges for alloying elements content [5], [11].

Element	Composition (%)
Chromium	0.2 – 0.6
Molybdenum	0.2 – 1.0
Vanadium	0.1 – 0.2
Nickel	0.6 – 1.0
Copper	0.5 – 1.5
Tin	0.04 – 0.08

Generally, all the alloying elements can be classified into three categories based on their graphitization potential and eutectoid transformations. From the alloying elements listed above, elements such as silicon and aluminum have a high positive graphitization potential for both the eutectic and eutectoid transformations that form solid solutions in the matrix. These elements reduce tensile strength and hardness due to the increasing ferrite/pearlite ratio.

In the next category, elements like tin, copper, and nickel have a high positive graphitization potential during the eutectic transformation but decrease the potential during the eutectoid transformation. The tensile strength and hardness are increased because of the higher pearlite/ferrite ratio.

In the last category, elements like chromium and vanadium, which are from the second part of the above list, have a negative graphitization potential at both transformation stages. Thus, they increase the amount of carbides and pearlites. These elements can form (FeX)nC – type of carbides (X is the alloying element) and alloy the αFe solid solution. As long as the carbide formation is eliminated, both tensile strength and hardness will increase [5], [11].

2.1.4. GCI Cooling Rate

Just like elemental composition, the cooling rate can significantly influence the mechanical properties of GCI. A well-designed wedge-shape GCI bar with about 10˚ taper of chemical composition of: carbon (3.52%), silicon (2.55%), Manganese (1.01%), phosphorus (0.215%), and sulfur (0.086%). The hardness readings were taken at an increasing distance from the tip to the bottom after the wedge-shape GCI was cast in a sand mold, as Figure 2.1-3 shown. The cooling rate decreases from tip to bottom due to the increase of size.

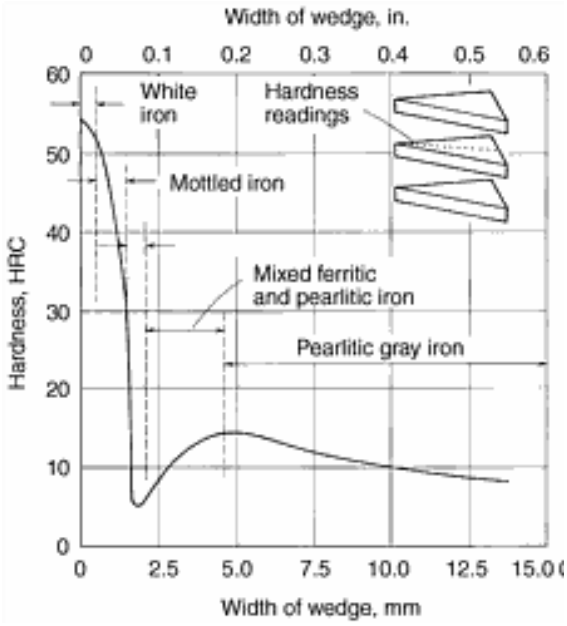

Figure 2.1-3 Influencing of cooling rate based on section size change. (based on [10]*)*

Considering the increasing width of the wedge as the cooling rate drops, the tip of the wedge has the most rapid cooling rate and thus forms chilled iron – white iron (a mixture of carbide and pearlite), which has a large amount of carbides and the highest hardness but reduced strength. With a slightly lower cooling rate (slightly increase width of wedge), the iron becomes mottled iron (a mixture of white iron and gray iron), and the hardness decreases dramatically. Minimum hardness is reached because of the occurrence of fine type D graphite flakes with a large amount of ferrite. A continuously

decreased cooling rate reaches another peak of maximum hardness on the curve. This is the most desirable structure due to fine type A graphite flakes with a pearlite matrix providing a balance of strength and hardness. Beyond this point on the curve, a lower cooling rate results in the formation of coarse graphite flakes in a pearlite matrix with relatively less hardness. Further decreasing the cooling rate, the pearlite matrix progressively decomposes into a mixture of ferrite – pearlite matrix, resulting in softer and weaker iron [10]. For a better understanding of this process, see Table 2.1 and Table 2.3.

Consequently, given the chemical composition, the cooling rate must be appropriately designed to provide the correct graphitization potential. The summary of the influence of chemical composition and cooling rate on the tensile strength can be estimated by equation 2.3 [5], [11].

$$\begin{aligned} \mathrm{TS} = 162.37 + \frac{16.61}{\mathrm{D}} - 21.78(\%\mathrm{C}) - 61.29(\%\mathrm{Si}) \\ - 10.59(\%\mathrm{Mn} - 1.7\%\mathrm{S}) + 13.80(\%\mathrm{Cr}) + 2.05(\%\mathrm{Ni}) \\ + 30.66(\%\mathrm{Cu}) + 39.75(\%\mathrm{Mo}) + 14.16(\%\mathrm{Si})^2 \\ - 26.25(\%\mathrm{Cu})^2 - 23.83(\%\mathrm{Mo})^2 \end{aligned} \qquad (2.3)$$

TS: tensile strength

2.1.5. Mechanical Properties

Typical phases found in GCI are: graphite, ferrite, pearlite, cementite, austenite, martensite, and steadite. Ferrite is the pure iron phase with low carbon content - it exhibits low strength but good ductility. Slow cooling rate and high silicon content promotes the formation of ferrite. Cementite, which is produced by a rapid cooling rate, is a very hard iron carbide (Fe3C) phase that significantly reduces the machinability or GCI. However, Pearlite, a product of alternate lamellar planes of soft ferrite and hard

cementite, provides an intermediate level of strength and hardness. The properties of pearlite are highly dependent on the interlamellar spacing (spacing between ferrite and cementite planes). The strength and toughness of the pearlite phase increases as the interlamellar spacing decreases. Austenite is similar to ferrite, as it is soft and possesses low strength. Martensite is formed by quenching high temperature austenite. It is extremely hard and notably difficult to machine. Eutectic phosphide (EP), is also known as Steadite. It is a hard-ternary eutectic phosphide system (Fe – Fe3C – Fe3P) forming at the end of the eutectic reaction due to its low liquid temperature [10], [17], [21]. More details are listed in Table 2.5.

Table 2.5: The influence of typical phases found in GCI on mechanical properties. (based on [5], [21])

Microstructure	Identity	Impact	Knoop Hardness 100gf (HK)
Graphite	Free-carbon phase Various sizes, shapes and distributions	Improves machinability Enhances damping properties Reduces strength	15–40
Ferrite (α – iron)	Iron with elements in solid solution Body-Centered Cubic	Provides ductility Low strength	215–270
Cementite (Fe_3C)	Iron carbide, hard intermetallic phase	Contributes to hardness and wear resistance Reduces machinability	1000–2300
Pearlite	Lamellar phase Ferrite + cementite Forms by a eutectoid reaction	Provides strength without brittleness Exhibits good machinability	300–390
Austenite (γ – iron)	Observed only in certain alloys Face-Centered Cubic	Soft and ductile Low strength	
Martensite	Produced by quenching an austenitic structure, typically by heat treatment	High hardness Brittle unless tempered	
Steadite	Iron-carbon-phosphorus ternary eutectic	Hard and brittle Aids fluidity when casting	600–1200

2.2. Age Strengthening

The first study of GCI age strengthening was published by R. Ebner in 1963 [22]. Later in 1999, Nicola and Richards reported that most classes of GCI exhibit age strengthening phenomena after being held at room temperature aging for over a month. The tensile strength of GCI increases from 3.3% to 13.5%. The rate of aging is highly time dependent and follows an Avrami-Johnson-Mehl curve shape, hence the rapid change of tensile strength can be observed in the initial days [23]–[25]. The previous authors were sponsored by the American Foundry Society with GCI testing bars produced in conformance to the ASTM A48 standard (test Bar B) [16]. Following over a month of room temperature aging, the results show a logarithmic curve in Figure 2.2-1.

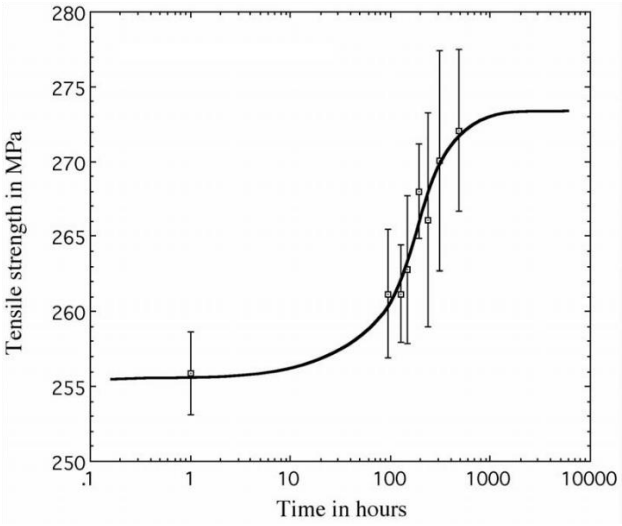

Figure 2.2-1 Room temperature age strengthening data over a month. (based on [26])

2.2.1. Effect of Aging Temperature

Artificial aging studies by Nicola and Richards [26] prove that temperature kinetically influences the rate of GCI age strengthening. One kinetic study with low holding temperature test was conducted by holding the test bars in a freezer at -16 ˚C in parallel with other samples aged at room temperature for 60 days. The results indicated a ninety percent confidence level that the test bars in the freezer fully aged after 60 days,

had a lower tensile strength compared to the test bars aging for the same amount of time at room temperature. Furthermore, samples that have been stored in dry ice resulted in halted aging.

On the other hand, test bars that were held at elevated temperatures (85˚C, 182˚C, and 285˚C) right after casting were compared with test bars aged 60 days at room temperature. Test bars with a lower temperature were immersed in a water bath at 85˚C, whereas other samples were held in an electrical resistance furnace at 182˚C and 285˚C.As Figure 2.2-2 shows, increasing temperature significantly accelerate the rate of age strengthening.

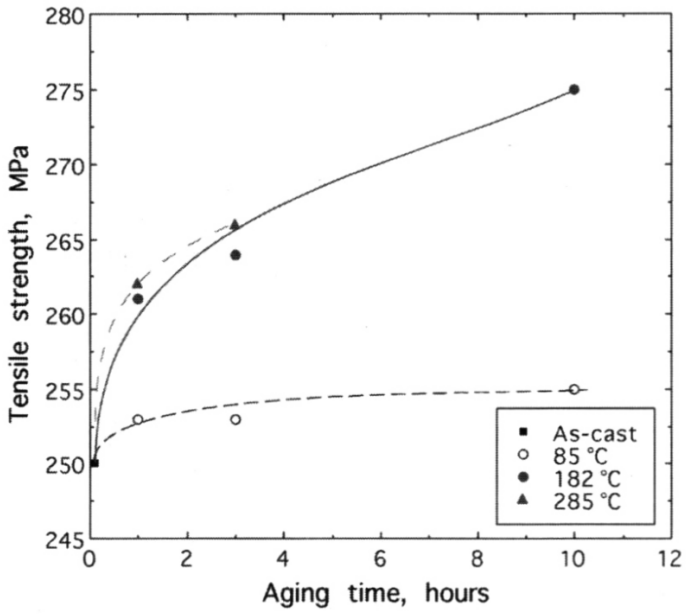

Figure 2.2-2 Acceleration of aging at 182 °C and 285 °C. (based on [26])

Further study by Richards et al shows that reverse aging can happen after fully aged test bars were exposed to 577˚C for 10 minutes or 704˚C for three seconds, which resulted in a drop of tensile strength of about 7% [27]. However, the aging process can be repeated by the reverse samples undergoing another sixty days of room temperature aging. Figure 2.2-3 is a brief summary of effect of aging temperature.

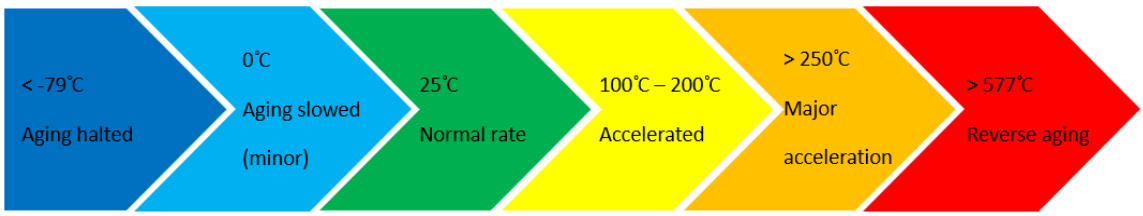

Figure 2.2-3 Influencing of temperature change on aging rate.

2.2.2. Effect of Nitride Precipitation

Age strengthening has been known as iron-nitride precipitation, and nitrogen is required to produce cast iron age strengthening behavior[26]–[32]. Stable Fe4N (also called: γ') and metastable Fe16N2 (also called: α'') are widely known as key factors of increasing the tensile strength after room temperature aging [33]–[42]. More specifically, Edmonds and Honeycombe [43] determined that a three-stage precipitation process, in which nitrides are precipitated into soft ferrite (α-iron), beginning with the formation of interstitial-atom clusters, followed by the nucleation of metastable Fe16N2 and ending up as the stable Fe4N [24], [44]. A heat treatment with the temperature below the iron-carbon eutectoid but beyond the iron-nitrogen eutectoid, can reverse the age strengthening process and reduce the increased strength [27]. This is the reason, shown in section 2.2.1, that the fully aged samples underwent reverse aging following a heat treatment with temperature above 577 ˚C.

2.2.3. Effect of Alloying Elements

As discussed above, GCI age strengthening is highly dependent on temperature and nitride precipitation. The artificial aging with elevated temperature accelerates the aging rate significantly; however, the natural aging at room temperature is strongly affected by GCI chemical composition. From section 2.1, manganese and sulfur are the most common and helpful alloying elements in GCI. The formation of MnS improves GCI machinability significantly. A result was published by S.N Lekakh and V.L. Richards [44] demonstrating that any free Mn element which does not form MnS, is likely to form the

nitride in the Fe-Mn-N system. The manganese iron nitride delays the sequential growth of the stable Fe4N and eventually appears as lower aging rate. [5], [11] provide the optimum ratio between manganese and sulfur for GCI, as shown in equation (2.4). Therefore, the calculation of free Mn is equation (2.5).

$$\%\mathrm{Mn} = 1.7(\%\mathrm{S}) + 0.15 \tag{2.4}$$

$$(\%\mathrm{Mn})_{\mathrm{free}} = \%\mathrm{Mn} - 1.7(\%\mathrm{S}) - 0.15 \tag{2.5}$$

Other elements such as Ti, Al and B strongly promote the formation of (X)nN – type of nitrides (X is the alloying element), which can easily suppress the iron nitride precipitation [28], [45]. Also, a carbide promoter such as chromium can decrease the amount of free ferrite in GCI as a cause of iron carbide formation. Since age strengthening, as a nitride precipitation phenomenon, happens in free ferrite, aging is eliminated without a traceable amount of free ferrite.

2.2.4. Influence of GCI Aging on Machinability

Usually, it is common sense that an increase in the hardness of the workpiece material also increases the machining cutting force, which leads to reduced machinability. Although aging increases the hardness and strengthening of GCI due to iron nitride precipitation, but it was proven by Edington et al. [31] that machinability actually improved from age strengthening of GCI and the result is shown in Figure 2.2-4. The total number of parts produced per cutting tool increases alongside the room temperature aging time. It is noticeable that the shape of the curve is logarithmic and similar to the increase of tensile strength along with aging time as shown in Figure 2.2-1.

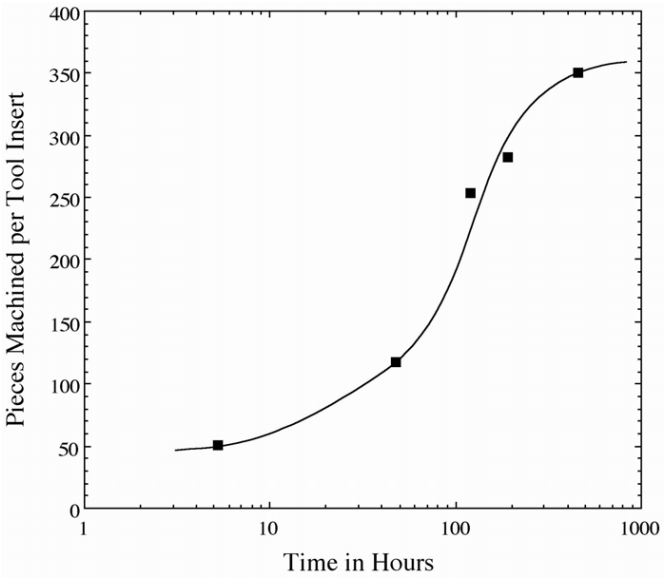

Figure 2.2-4 Effect of GCI aging on machinability. (based on [31])

This unusual behavior is due to the reduction of energy consumption during the chip formation process. Although GCI possesses a poor tensile strength and good compression strength, it requires high energy for plastic deformation. Even worse, soft free ferrite in un-aged GCI absorbs too much energy for chip formation and the free ferrite is too soft compared to other phases of iron. It generates a built-up layer on the tool insert and further increases the cutting force. The iron nitride precipitation in free ferrite helps to increase the hardness as well as the strength of the soft free ferrite and contributes to less energy requirement for chip formation, therefore reducing the cutting force and improving the machinability.

Results provide by S.N Lekakh and V.L. Richards [44] show that the dependency in which the cutting force decreases in reverse proportion to the hardness, is only due to age strengthening of GCI in each sample iron. As Figure 2.2-5 shows, heat 2, heat 3, and heat 4 are the four foundries of GCI chosen by authors. Full aging of GCI contributes to an increase of Brinell Hardness and a significant reduce of the average cutting force.

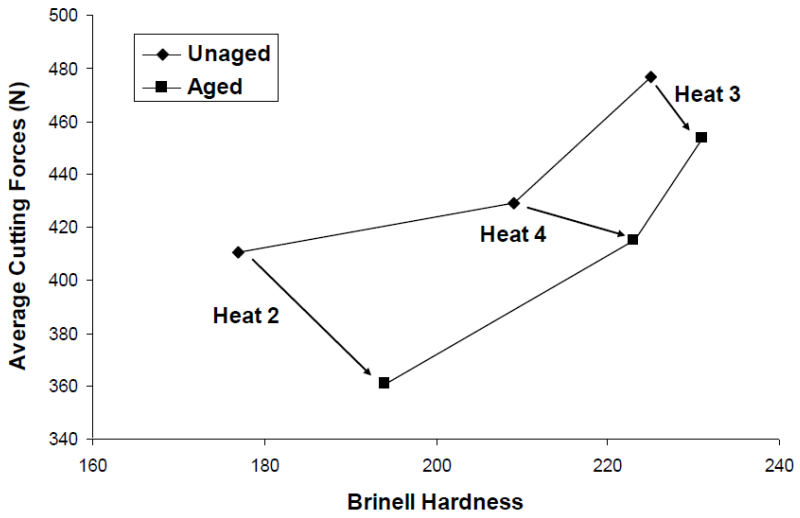

Figure 2.2-5 Dependency of cutting force with hardness by aging. (based on [44]*)*

2.3. High Speed Machining

High speed machining (HSM) is a technology of cutting material under a high cutting speed. This High Speed Cutting technology was first studied by its inventor, C. Salomon since 1931 [46]. There is no absolute definition of HSM based on different application requirements and different authors. However, the major objectives of HSM research can be classified into three categories. In the beginning, the motivation of studying HSM was the search for a technological breakthrough in the machining of difficult-to-machine materials, such as superalloys, titanium alloys, hardened alloy steels and etc.. The cutting speed used for these tough materials is still limited by the tool wear. The second goal is to achieve high surface quality and better machining accuracy, in which HSM has been successful in many applications and usually at finish cutting of material. Lastly, the finishing process usually takes a comparatively long time and manufacturers strive to get higher productivity while reducing the production cost and increasing the production efficiency. Due to the last goal, HSM has become more favorable in modern machining technology [47]. In 1992, H. Schulz and T. Moriwaki [47] describe the following advantages of HSM over the conventional cutting process:

- Increased machining accuracy, especially in machining of thin webs due to reduced chip load
- Better surface finish and reduction in the damaged layer
- Reduced bur formation
- Better chip disposal
- Possibility of higher stability in cutting due to stability lobes against chatter vibration
- Simplified tooling, and etc.

Different workpiece material at different applications have a different range of cutting speed for HSM, as shown by Figure 2.3-1.

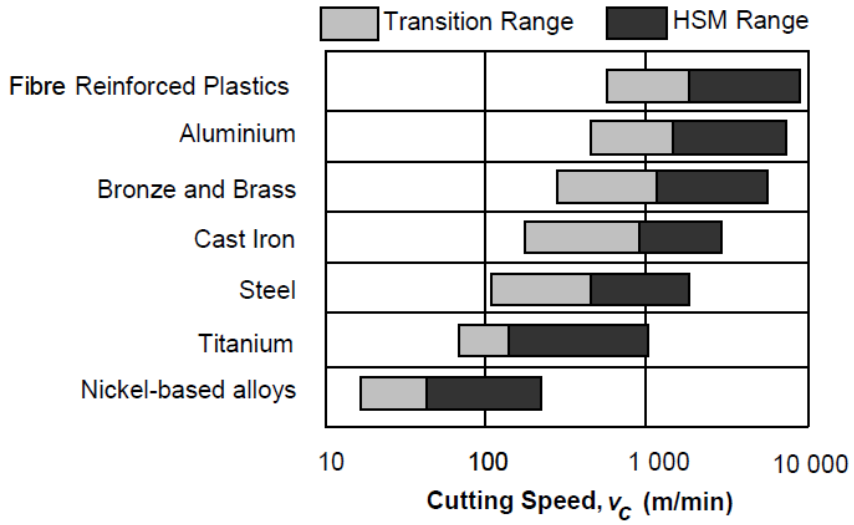

Figure 2.3-1 Different range of cutting speed for HSM. (based on [21], [47]*)*

2.3.1. Tools for HSM of GCI

Hard metals with and without a coating layer [48]–[50], cermet and ceramic tool inserts [51]–[55], and last but not least polycrystalline boron nitrides also known as CBN or PCBN [3], [56] are mostly used for HSM of steel and cast iron due to their good wear resistance under severe cutting conditions.

However, in many applications, it was realized that even carbide or ceramic tools struggle to meet the strict manufacturing requirements. Manufacturers eagerly demand critical elements in metal cutting with sufficient tool wear resistance and less production cost while the workpiece materials are becoming harder, tougher, and more chemically reactive. Researchers found that the CBN cutting tool is the best candidate for HSM.

CBN is the second hardest material after diamond, possessing high thermal conductivity and excellent chemical stability at high temperatures. These characteristics make CBN, as a cutting tool, perfectly fit the requirements of HSM. Although CBN cutting tools are very expensive compared to other conventional carbide or ceramic tools, optimizing the cutting conditions can maximize the production efficiency. Just like carbon, they exhibit a soft, slippery hexagonal structure called graphite well as a cubic structure known as diamond. Boron nitride (BN) has a soft hexagonal boron nitride (HBN) structure which can be transformed into a cubic boron nitride (CBN) structure under high temperature and pressure. Figure 2.3-2 from [57] shows the transformation.

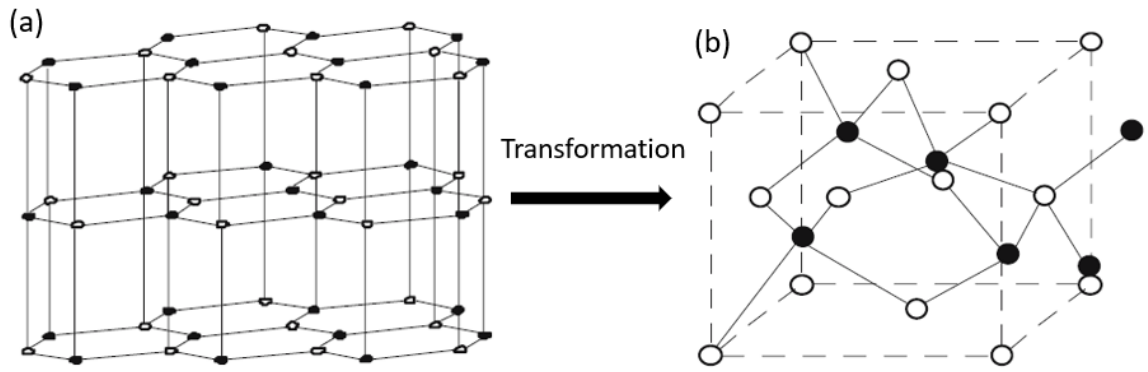

Figure 2.3-2 Two structures of boron nitride: (a) is HBN, (b) is CBN. (based on [57]*)*

The most common types of CBN available on the market can be classified into two categories. One category is cutting tools possessing around 0.9 volume fraction of CBN grains with metallic binders such as cobalt, defined as high CBN content tools. The other category usually has around 0.5 to 0.7 volume fraction of CBN grains with ceramic

binders such as titanium nitride or titanium carbide and is defined as low CBN content tools [57]. Takatsu et al. [58] reported that the CBN tool life is mainly related to flank wear and chipping on the cutting edge. The flank wear is influenced by both the inherent wear resistance of the CBN compacts and the adhesion of the workpiece materials [57].

2.4. Metal Cutting Process

The chief activity of industry around the world revolves around shaping materials into desired parts. This is also known as the process of metal cutting, in which the unwanted materials are removed from the workpiece by a variety of traditional chip removal processes such as turning, milling, drilling, and boring. In other applications, abrasive processes such as grinding and honing, as well as nontraditional machining processes such as electro-discharge machining (EDS), ultrasonic machining, laser machining, water jet machining, and electrochemical machining are related to metal removal processes [59].

2.4.1. Orthogonal Cutting

Since metal cutting processes are complex, in order to get a better understanding of cutting process, two cutting models of “orthogonal” and “oblique” cutting are carried out for physical analysis. Figure 2.4-1 shows these two cutting models in which the orthogonal cutting is uniform in the direction perpendicular to the cutting, while the oblique cutting is not uniform.

Most of the time, the 2D shear plane model of orthogonal cutting is used for studying the machining processes. The model was firstly proposed by V. Piispanen [60], [61], Ernst [62], and Merchant [63]–[65].As Figure 2.4-2 shows, they assumed that chip formation shearing occurs along a single plane which makes a shear angle (ϕ) with respect to the machined surface. This simple model is useful to analyze the mechanics of metal cutting such as cutting forces and chip formation.

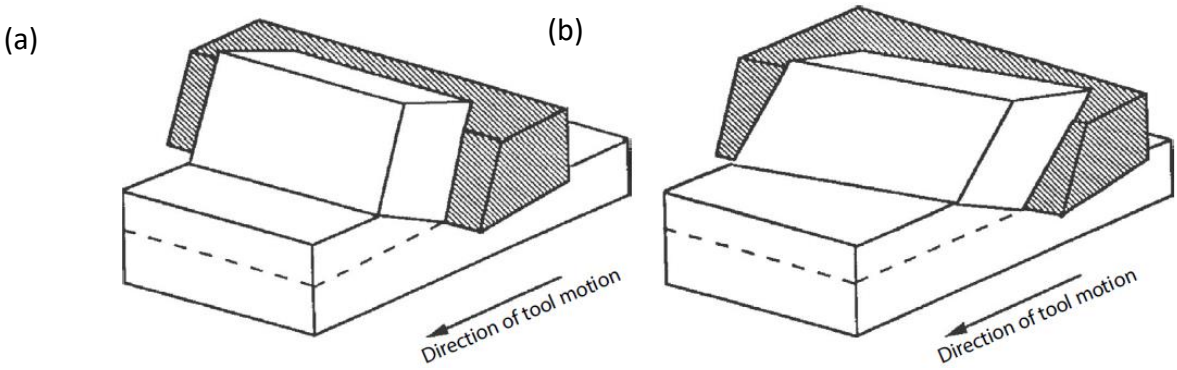

Figure 2.4-1 (a) is orthogonal cutting and (b) is oblique cutting. (based on [59]*)*

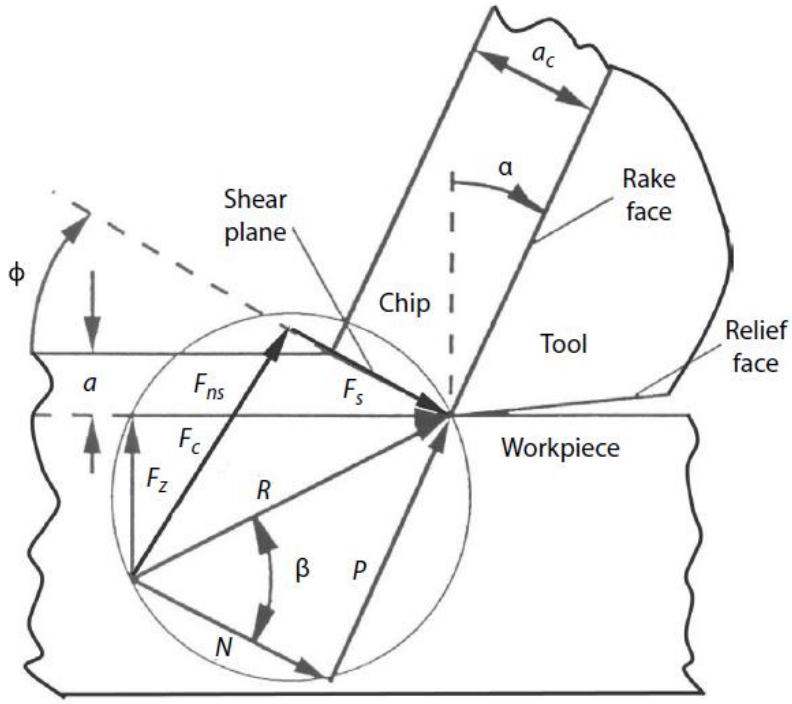

Figure 2.4-2 Ernst and Merchant's shear plane theory of orthogonal cutting. (based on [59]*)*

2.4.2. Turning

This GCI machinability research is in accord with the industrial partner's cutting setup for collecting representative data. A high-speed turning process is the chosen metal cutting operation. Figure 2.4-3 shows the cutting mechanism of turning.

The turning process is traditionally carried out with a lathe. In turning, a cutting tool feeds into a rotational workpiece to generate an internal or external surface.

High cutting speed turning [59], [66], is usually machined with carbide, ceramic or CBN tool inserts. In machining hardened materials such as GCI in this study, high speed turning provides more potential advantages than conventional turning, such as less production cost, less operation steps, higher production efficiency, and the elimination of cutting fluid. Under intensifying cutting conditions, a CBN tool enables the high speed turning technology to potentially replace the grinding process[57], [67]. It has been noticed that the stripped hard boron nitride particles easily generate three-body abrasive wear on the tool flank face. This flank wear is a major limitation of CBN tool life during high speed turning [67].

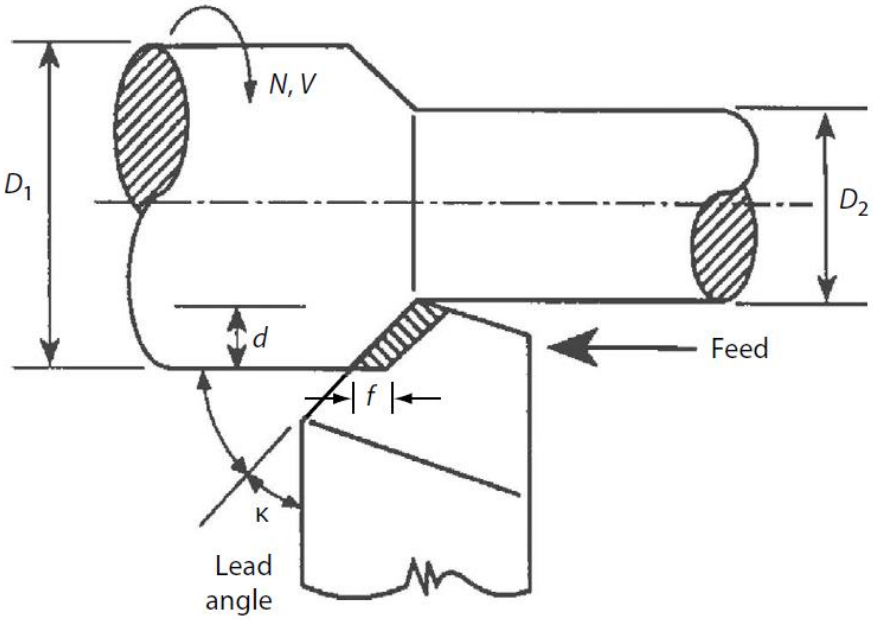

Figure 2.4-3 Simple turning model. (based on [59])

2.4.3. Tool Wear Mechanisms

Tool wear and tool failure directly influence the manufacturing costs and production quality. A longer tool life or a high tool wear resistance are always desired by researchers and engineers, which contributes to less production costs, more consistent production quality and better surface finish. It is important to understand the different

types of tool wear and their causes. The principal types of tool wear are shown in Figure 2.4-4, and the detailly discussion of each type of tool wear is shown in Table 2.6

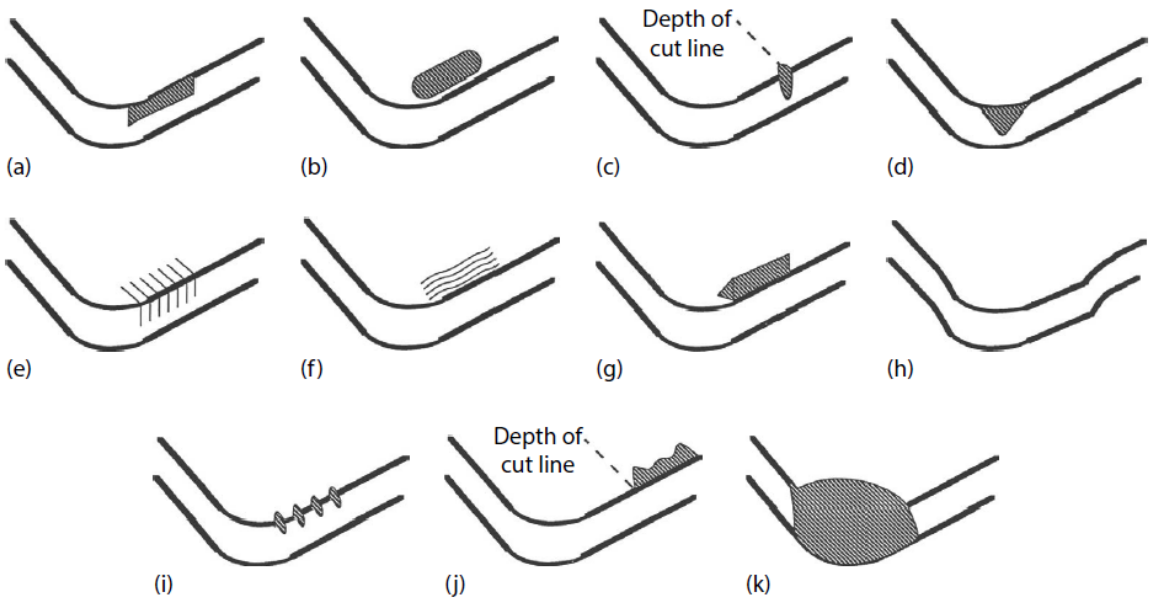

Figure 2.4-4 Types of wear on cutting tools: (a) flank wear; (b) crater wear; (c) notch wear; (d) nose radius wear; (e) edge (thermal) cracks; (f) parallel (mechanical) cracks; (g) built-up edge; (h) edge plastic deformation; (i) edge chipping or frittering; (j) chip hammering; (k) gross fracture. (based on [59]*)*

Flank wear, being easy to measure, is usually taken in many applications to represent tool life. The formation of wear land on the tool flank face increases the contact area between the tool and the workpiece, which generates greater friction heat and cutting forces, eventually leading up to a poor dimensional accuracy. An ideal flank wear rate varies with time as Figure 2.4-5 shown. The initial rounding of the cutting edge causes a rapid wear rate of the fresh tool, followed by a steady rate of flank wear until the wear land reaches a certain length and another case of severe flank wear occurs.

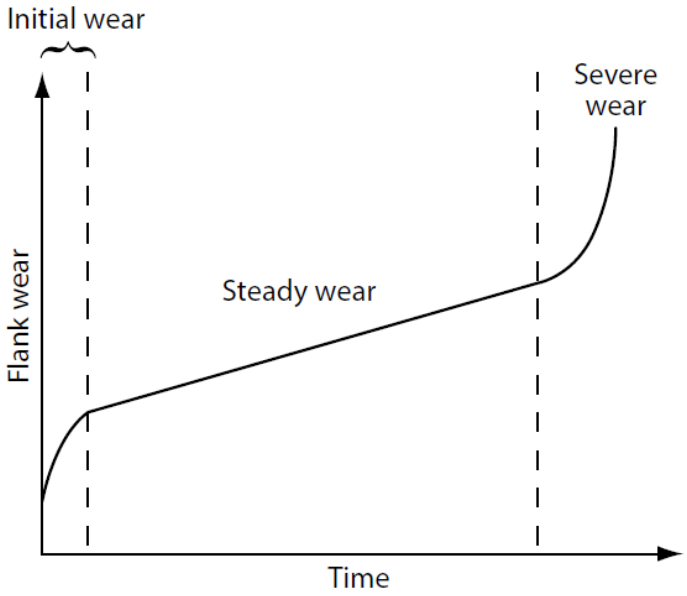

Figure 2.4-5 Ideal variation of the flank wear rate with cutting time, showing the initial wear, steady wear, and severe wear periods. (based on [59]*)*

Table 2.6: Tool wear mechanisms and characteristics. (adapted from [59], [68])

Type of Wear	Mechanism	Characteristics
Flank Wear	Abrasion	Caused by rubbing of the flank face on the machined surface
Crater Wear	Diffusion Adhesion	At elevated temperatures the tool material will begin to diffuse into the workpiece material causing craters to form; alternatively, the craters may form due to micro-chipping as tooling layers are sheared away by localized adhesion effects
Notch Wear	Oxidation	This wear type typically occurs in turning or other processes where the majority of the tool is continuously embedded in workpiece material and therefore not exposed to oxygen in the surrounding atmosphere. However, at the depth of cutting line the tool is exposed and the elevated tool temperatures cause notch wear to form due to oxidation along that line
Nose Wear	Abrasive Oxidation	Nose wear typically occurs in turning operations on the relief face of the tool and is a combination of flank wear and notch wear. The relief face allows oxygen to reach near to the cutting-edge allowing oxidation wear to occur in addition to abrasive wear resulting in flank wear

(Continued)

Table 2.7: Tool wear mechanisms and characteristics. *(Continued)*

Type of Wear	Mechanism	Characteristics
Edge Cracking	Mechanical (Thermal)	In brittle tools, temperature gradients developed on the cutting tool may cause thermal stresses on the surface of the tool which will can cause or accelerate cracking of the tool or coatings
Parallel Cracking	Mechanical	Especially prevalent in interrupted cutting such as milling, mechanical cracking may occur in brittle tools due to impact loading on the tool's cutting edge. Repeated impacts initiate crack propagation which weaken the cutting edge of the tool and may lead to chipping or gross fracture
Built-up Edge	Adhesion	Due to high temperature and loads occurring in the cutting zone, workpiece material can weld to the tool. If the degree of adhesion is large, the tool material may build up on the tool's cutting edge, effectively increasing the size of the tool. Eventually the built-up edge will reach a critical size, at which point it may break away harmlessly, or may fracture a large piece of tool material, often resulting in tool failure
Edge Plastic Deformation	Mechanical	This type of wear is most common in ductile tooling materials, such as high-speed steel. Due to high heat and loading, the tool material may deform, changing the tool geometry, depth of cut and other important process parameters
Edge Chipping	Mechanical Abrasive	Edge chipping can be the eventual result of residual cracks caused by either thermal (comb cracking) or mechanical (parallel cracking) wear types, and is especially prevalent in interrupted cutting, such as milling. It can also be the result of adhesive wear, were the level of adhesion is small and so fractured tool material remains minimal
Chip Hammering	Mechanical Abrasive	Chip hammering occurs when the formation of the chip is not well controlled. The chip curls up, away from then tool and is then forced back down to strike and abrade the tool away from the cutting zone
Gross Fracture	Mechanical Adhesion	Catastrophic failure of the tool by massive chipping/gross fracture can occur for a number of reasons. If mechanical loading on the cutting edge far exceeds the capacity of the tool to support it can cause this. As well, the breaking off of a large built up edge can cause gross fracture as previously discussed. Severe thermal or mechanical cracking can also lead to this wear mechanism

Chapter 3: Experimental Work

The MMRI is one of the largest university-based manufacturing research institutes in Canada, supporting academic research and education programs that span many manufacturing processes. The institute's core focus is to enhance productivity, quality and product/process innovation while helping companies reduce costs. The purpose of this major industrial funded research project is to achieve a better understanding of the variation of GCI machinability. Resources allocated to this s project cover multiple Master and PhD students' research works starting from 2015. The tests conducted cover multiple academic fields with wide support provided by MMRI staff and researchers.

The research engineer, Ahmed Sweed at MMRI helped to optimize and finish the machinability tests of the GCI age strengthening phenomena. He also conducted a machinability test to optimize the different options available for CBN cutting tools.

Bipasha Bose is the PhD material engineering specialist at MMRI. Her parallel nano-indentation tests helped increase GCI hardness after room temperature aging.

3.1. Workpiece Materials

The GCI workpiece materials were supplied by our industrial partner, which is the FC250 grade of GCI cylinder sleeves shown as in Figure 3.1-1. For cross reference, please check Table 2.2. The GCI sleeves were used for high speed turning preliminary tests followed by the study of the cutting speed's effect on CBN tool wear behavior and the study of varied CBN composition wear behavior. The cutting condition and the appropriate CBN cutting tool were chosen based on the results obtained from the preliminary tests.

Figure 3.1-1 GCI engine sleeves.

3.1.1. Workpiece Material Characteristics

Basic information of modified FC250 GCI cylinder sleeves were provided by the industrial partner. Table 3.1 shows the characterization of the workpiece material, such as chemical composition, microstructure, and mechanical properties.

Table 3.1: Workpiece material characterization of modified FC250 GCI cylinder sleeves.

Mechanical Properties	**Tensile Strength (N/mm^2)**	**Rockwell Hardness (HRB)**
	250 min	Around 98
Microstructure	**Matrix**	**Graphite**
	Predominantly pearlitic Small amounts of free ferrite & steadite	Major type A Minor type B & D
Chemical Composition (wt. %)		
C: 3.20 – 3.50	Si: 1.70 – 2.20	Mn: 0.60 – 0.90
P: ≤ 0.15	S: ≤ 0.10	

3.1.2. Metallographic Analysis

From the second half of 2015, the industrial partner has been collecting and providing sleeves to MMRI on a bi-weekly basis. The goal was to establish a timeline of

microstructure information, which could be tied to periods of poor machinability as described in the introduction. Observations of free ferrite content and aging phenomena also require metallographic inspection of the samples to record the change of material characteristics. Metallographic analysis was carried out on small pieces of GCI workpiece cut from individual cylinder sleeves by bulk abrasive saw and hot-mounted in an epoxy resin with mineral filler using Struers Ensuring Certainty Hot Mounting under a temperature of 150˚C and pressure of 250 Bar for 5 mins of heating and 3 mins of cooling. All the mounted samples were then ground using progressively finer grades of SiC paper (P500 – P4000) and polished with a final 1µm diamond particle and "blue-ethanol" lubricant mixture with a Struers Ensuring Certainty Auto-polisher. After each progressively finer step of polishing, especially at the final step, samples were rinsed in 95% ethanol and dried using a hot air blower. Polished samples were examined with a Nikon optical microscope. Unetched sample's image is shown as Figure 3.1-2.

To further understand the microstructure of GCI and the results of quantitative image analysis, samples were finally etched with a mixture of 2% HNO3 with 98% DI water (2% Nitro) to the polished surface for approximately 15 seconds. The samples then underwent the same cleaning and drying procedure as during image examination polishing, see Figure 3.1-3.

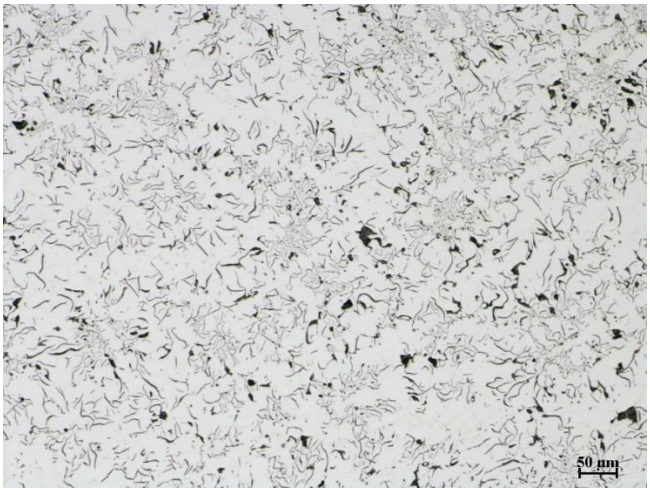

Figure 3.1-2 A sample of unetched microstructure of FC250 GCI with a magnification of ×100.

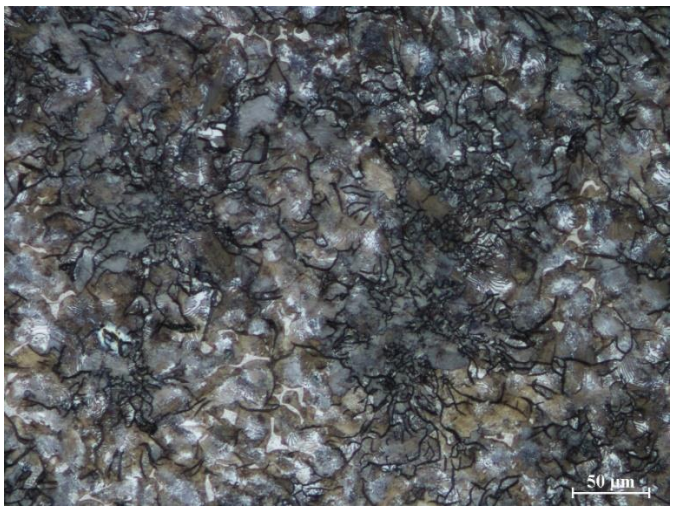

Figure 3.1-3 A sample of etched microstructure of FC250 GCI with a magnification of ×200.

3.1.3. GCI Skin Layers

Following the initial metallographic analysis of the GCI microstructure, it was discovered that the outside surface of the cylinder has a different microstructure than the bulk or main body material. There is no universal definition of the GCI skin region, and the type of graphite structure in this region is a variety of type D and E graphite instead of the type A structure. The matrix in this skin region is predominantly ferritic with small amounts of pearlite and carbide. As author Jared Teague refers in his thesis, the short layer of predominant free ferrite with a highly undercooled graphite is attributed to the short distance it takes for the matrix carbon to diffuse into graphite flakes. Therefore, the austenite phase forms the stable ferrite phase instead of transforming into metastable pearlite phase [27], [69].

In Figure 3.1-4, the difference of microstructure between the outside skin layer and the main body can cause a significant increase of CBN tool wear. To avoid the influence of the skin region, all GCI cylinder sleeves were pre-machined with separate cutting tools to remove the skin layers. All the optical microstructure images were taken from the bulk material to maintain the consistency.

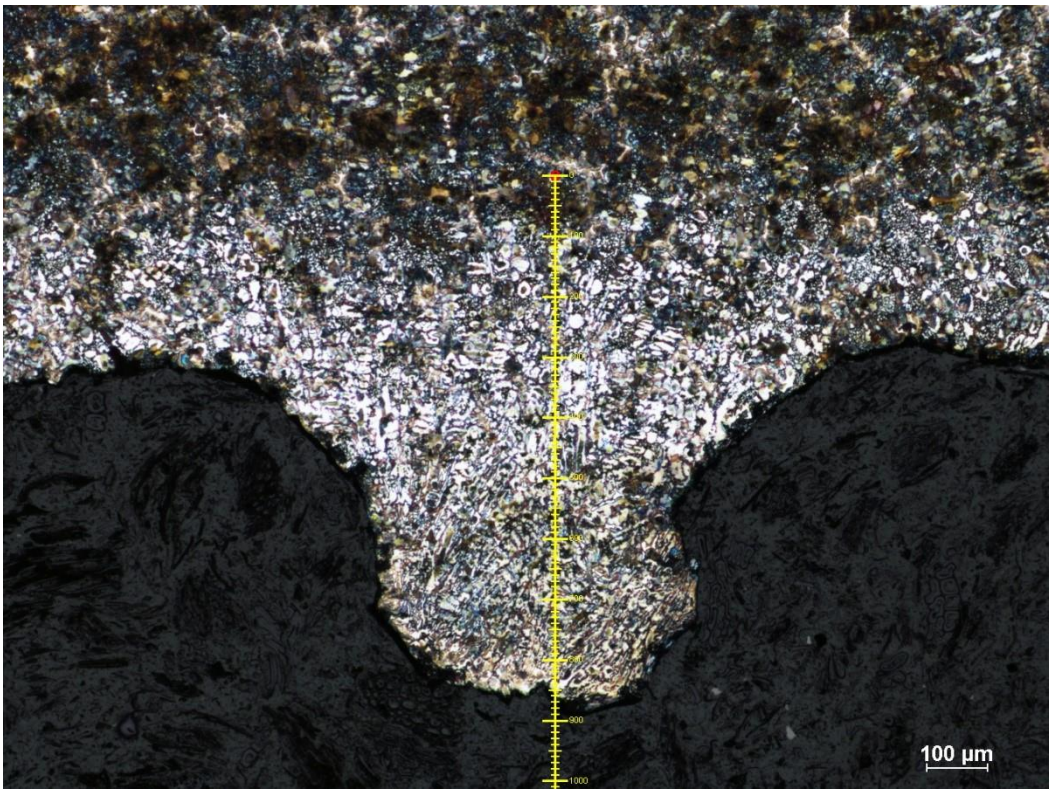

Figure 3.1-4 Skin region with predominant free ferrite. The maximum thickness for the layer is around 1mm.

3.1.4. Scanning Electron Microscopy

Scanning electron microscopy (SEM) was used to further confirm the composition of elements within the GCI microstructure and to analyze the detail of cutting tool wear behavior. The MnS inclusions found by SEM, see Figure 3.1-5 show the EDM mapping on local points with sharp crystal inclusions. The atomic mass of manganese is 55 and the atomic mass of sulfur is 32. The EDS analysis shows the Wt% of manganese to be 57.5 and sulfur 33.8, a ratio is very close to the standard 55:32, proving that the sharp inclusions are MnS.

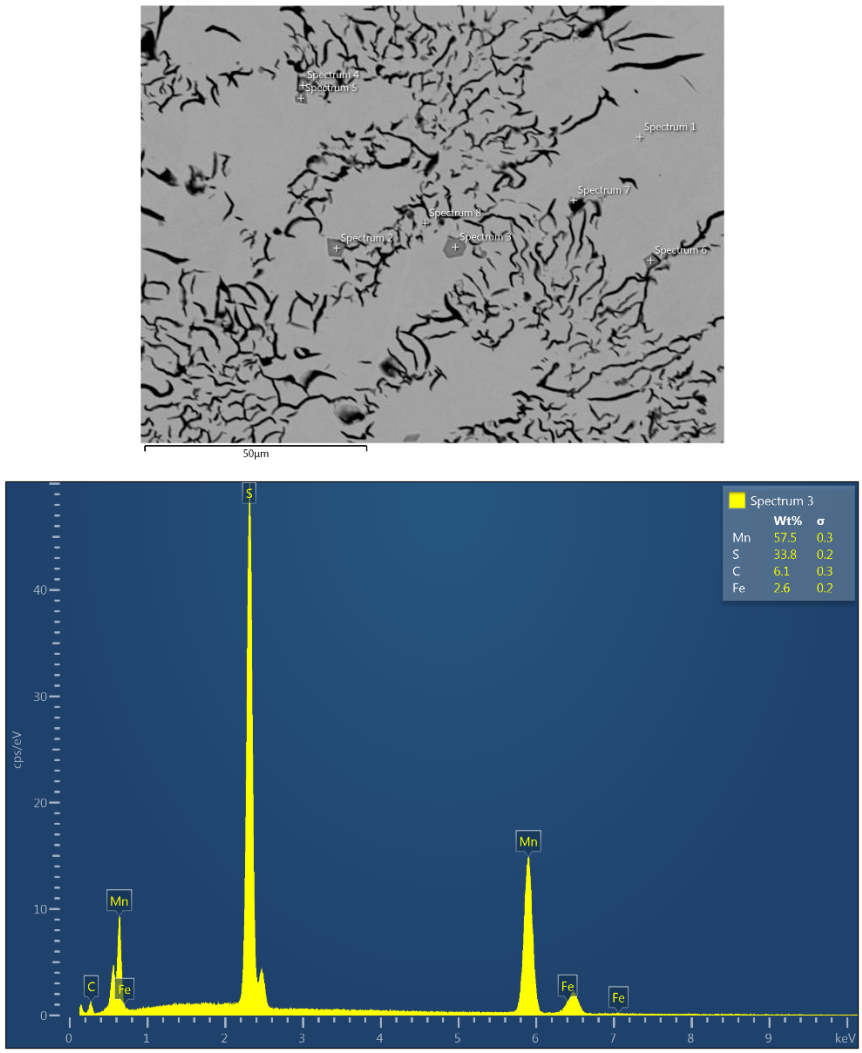

Figure 3.1-5 EDS mapping with results show the sharp crystals are MnS inclusions.

3.1.5. Quantitative Image Analysis

Etched optical microscope images are analyzed using QIA (quantitative image analysis), ImageJ computational programs that have built in features for image processing and analysis. This software identifies “free ferrite” pixels (red), counts them, and then divides them by the total number of pixels in the image, providing %area result. The software operates on user-specified thresholds for which pixels should be counted. QIA cannot differentiate between free ferrite and steadite as they are similarly colored. See following Figure 3.1-6. The advantage of QIA is that it can differentiate between different

materials based on the color contrast. However, the result is subjective, since the red area is a manual threshold which may underestimate or overestimate the reading. Also, since steadite and free ferrite have a similar color, a small amount of steadite is present in the result under any color contrast. However, its influence is negligible.

On the other hand, there is no exact measurement of free ferrite which can only be optimized. To get a relatively reliable result with QIA, the optimized threshold between the higher and lower estimate was chosen from the average of multiple images.

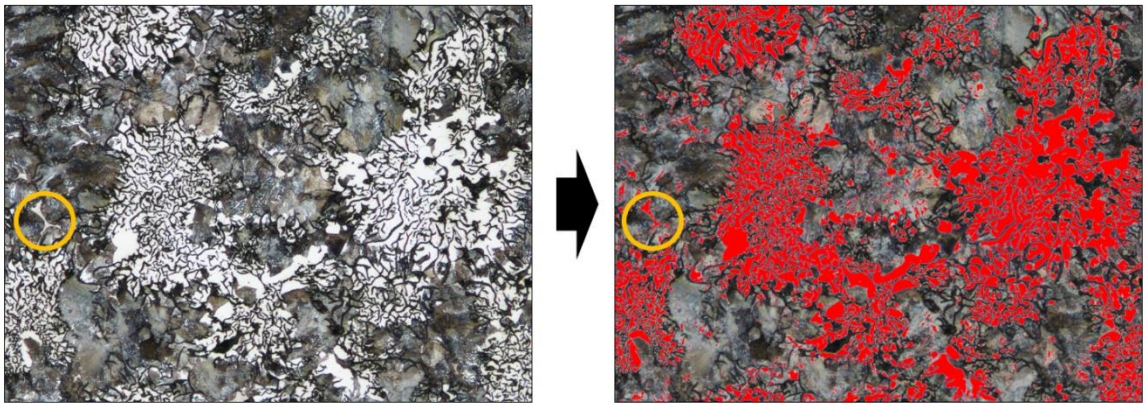

Figure 3.1-6 Quantitative image analysis by ImageJ, the red area is free ferrite based on the pixels been counted. Yellow circle is steadite which been counted as free ferrite.

3.2. Cutting Tools

Four indexable CBN cutting inserts were mounted in a commercial tool holder for high turning to study the variation of GCI machinability for the cutting process optimization. The geometries of these inserts are constant, see Table 3.2.

Table 3.2: Cutting inserts information.

Insert Grade	CBN (vol%)	Grain Size (µm)	Chamfer	Rake Angle	Major Binder
Composition 1	95	2	No Chamfer	0˚	Titanium Alloy
Composition 2	85	2	No Chamfer	0˚	AlWCoB
Composition 3	65	3	No Chamfer	0˚	TiN
Composition 4	50	1.5	No Chamfer	0˚	TiC

3.3. Experimental Setup

All of the experimental tests were conducted such that material, machine, tool and process factors mimic actual industrial production conditions as close as reasonably possible. The setup used in testing is described below, see Figure 3.3-1. Different cutting conditions are listed in the beginning of each new section.

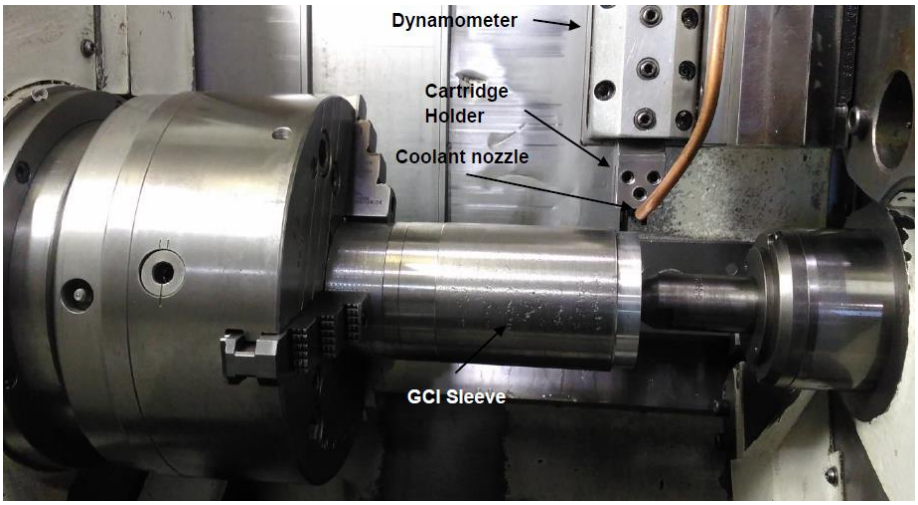

Figure 3.3-1 Machine setup.

The total sufficient cutting length by one GCI cylinder sleeve is limited to a range of around 2500 m to 3000 m due to the wall thickness. Under the high-speed turning process, a sufficient cylinder wall material thickness is significantly important, since the vertical cutting force can eventually break the workpiece via incremental increases of the cutting depth towards the center of the cylinder. In this case, a pre-machined workpiece metal holder and hat was used to help clamp and support the cylinder sleeve, but nonetheless, for the safety reasons, the maximum cutting length a cylinder sleeve may reach is around 1000 m.

The cutting force (F_c), feed force (F_f), and radial force (F_d) are measured using a three-components dynamometer as shown in Figure 3.3-2. It consists of four three-component force sensors, with each sensor containing three pairs of quartz plates, one sensitive to pressure in the Z direction and the others responding to shear in the X and Y

direction respectively. The measuring circuit consists of a dynamometer, amplifier, data acquisition card and computer.

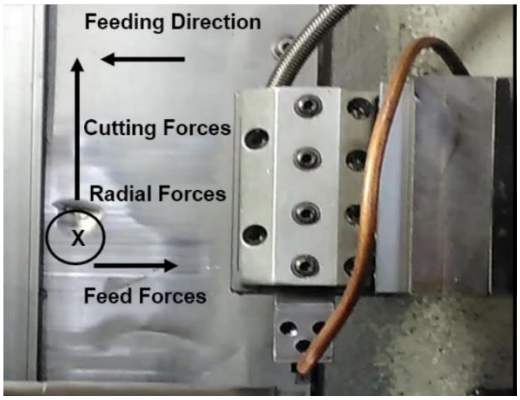

Figure 3.3-2 Dynamometer with cutting forces directions.

Chapter 4: Tool Wear Behavior of Varied CBN Composition

4.1. Experimental Procedure

Tests on the tool wear behavior of four types of CBN cutting tools, as shown in Table 3.2, were conducted to optimize the following machinability tests and to observe how different machining process parameters and tools performed under given material conditions. The data for these four CBN cutting inserts are shown in Table 3.2The major differences between them are the volume percentage content of CBN particle, the CBN particle size, and the binder materials.

The experiments were conducted on BOEHRINGER VDF 180 CM CNC turning center with Siemens controlling unit using a pre-machined (skin layers were removed) cylindrical GCI sleeve. All the workpiece materials were fully aged and QIA was performed prior to running the machining processes, so that all of the workpieces had similar microstructure and mechanical properties. The machine setup is the same as Figure 3.3-1 described. Detail cutting conditions are listed below.

Cutting Speed:	1176 m/min
Feed Rate:	0.125 mm/rev
Depth of Cut:	0.3 mm on radius
Cutting Fluid:	Flood coolant, semi-synthetic, 8-10% concentration
Tool Failure Criteria:	300 µm length of flank wear

All cutting conditions were chosen to simulate those found in industry, in order to get relatively reliable results. As section 2.4.2 mentioned, CBN inserts are extreme hard cutting tools best suited for the high-speed turning process, but the stripped CBN particles easily cause abrasive wear on flank face. In industry, a 300 µm length of flank wear is a common failure criterion to indicate tool life. Whenever significant tool chipping occurs or the flank wear reaches 300 µm, the machine processes would stop and the total cutting length for each type of CBN tool would be calculated and listed as a graph.

$$\text{Cutting Length} = \sum_{i=1}^{n} (\pi \times D_i \times \text{Z})/(1000 \times \text{f}) \tag{4.6}$$

D_i: uncut diameter of cylinder sleeve at i cutting pass; **Z**: cut length of cylinder sleeve; **n**: total number of cutting pass per insert; **f**: feed rate

4.2. Results and Discussion

The cutting tool optimization tests were conducted with four different types of commercial CBN inserts with fully aged GCI workpiece materials of FC250 grade. These four CBN inserts are CBN composition 1, composition 2, composition 3, and composition 4 with details listed in Table 3.2. The content of free ferrite is less than 2% for this batch of workpiece material. The cutting condition for these four different types of CBN inserts were constant according to the industrial partner's cutting parameters. Using a BOEHRINGER VDF 180 CM CNC turning center, the cutting speed was 1176 m/min, depth of cut on radius is 0.3 mm per pass, and the feed rate is 0.125 mm/rev. As mentioned in section 3.1.3, the GCI cylinder sleeves have a 1mm thick ferritic skin layer, and following the removal of this layer on all the workpiece materials, the maximum cutting passes are limited to a total of four on each cylinder sleeve. Under severe cutting conditions of HST, the reduced cylinder sleeve wall thickness can cause critical damage from friction with the workpiece. Each different cutting pass has a different uncut diameter of the cylinder sleeve and the total cutting length can be calculated with equation 4.6.

In industry, it is common to set the tool failure criteria to 300 µm length of flank wear. The following optical microscopic images Figure 4.2-1 show the wear behavior on both flank face and rake face of four chosen CBN cutting tools, after each insert reaches its tool failure criteria. The total tool wear behavior graph and tool wear pattern is shown in Figure 4.2-2.

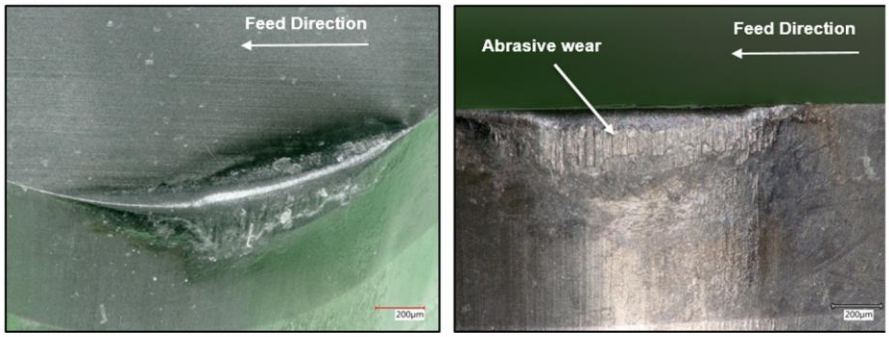

Optical images of CBN cutting tool with composition 2 after cutting length of 104620 m

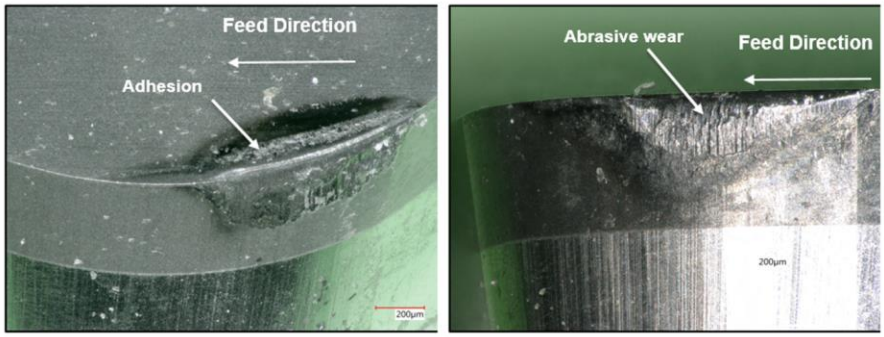

Optical images of CBN cutting tool with composition 1 after cutting length of 59428 m

Optical images of CBN cutting tool with composition 3 after cutting length of 29565 m

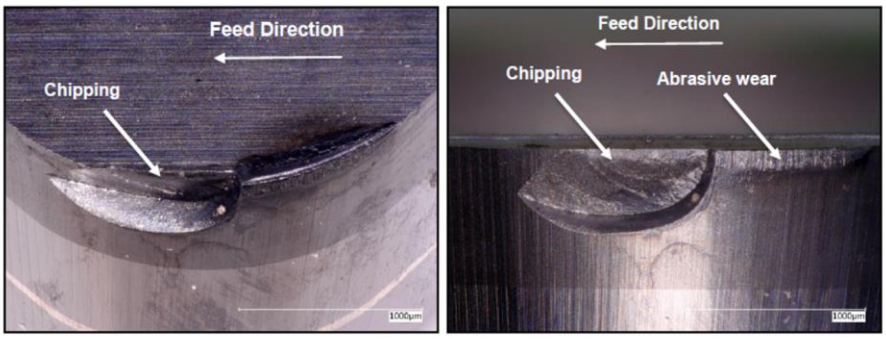

Optical images of CBN cutting tool with composition 4 after cutting length of 5243 m

Figure 4.2-1 Optical Microscopic images of CBN inserts "CBN composition 1, composition 2, composition 3, and composition 4" after flank wear reaches 300 µm.

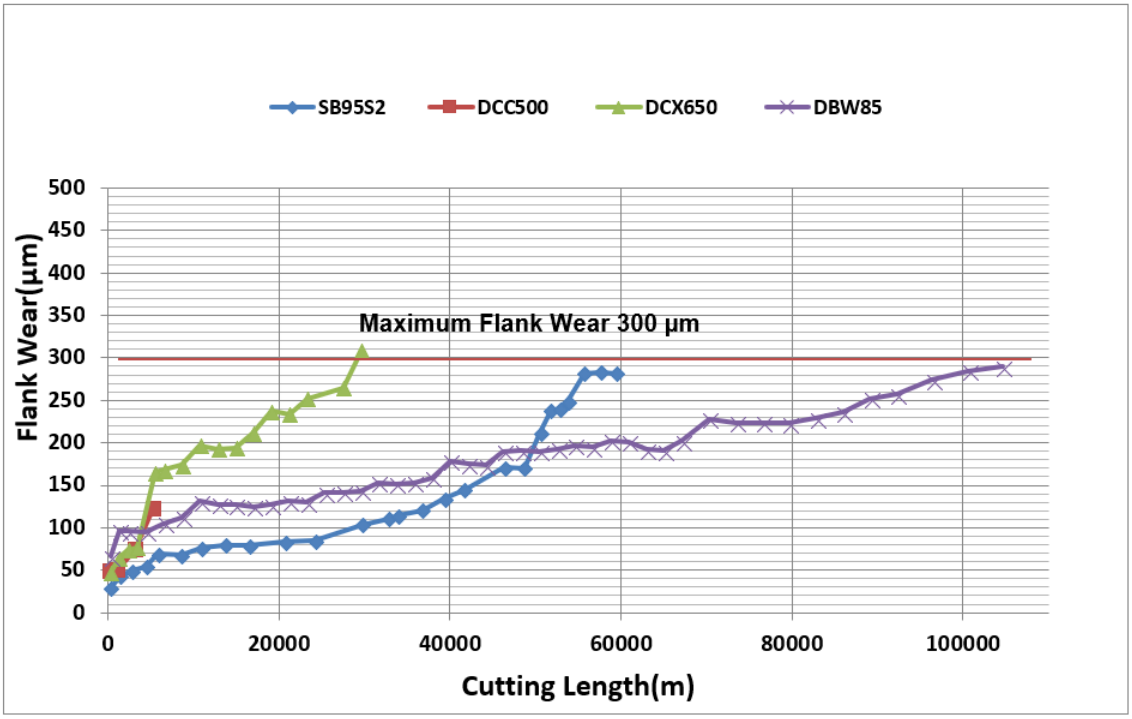

Figure 4.2-2 The total cutting length of each type of CBN insert after flank wear reaches 300 µm.

It is observed that the major tool wear progress of the CBN cutting tool 1, 2 and 3 is abrasive wear on the tool flank face, and for the CBN 4 cutting tool, it is massive chipping. The existing flank wear on the flank face was caused by the abrasion of peeled CBN particles, evident from the groove marks clearly seen on the entire CBN flank face.

The most common wear behavior of CBN cutting tools is abrasive wear [67], and the CBN cutting tool with composition 4 has massive chipping after 5,243 m length of cutting. Jiancheng Liu and Kazuo Yamazaki's study [2] mentions that the CBN insert with a TiC binder and moderate % content of CBN particles and large CBN particles provides the best tool wear performance from a list of selected CBN cutting tools. As a result, the chipping on the CBN 4 is due to the fewer % content of CBN particles and their small size, which results in low chipping resistance.

The rest of the CBN cutting tools feature good tool life under severe cutting conditions. Prior to a 50,000 m length of cut, CBN composition 1 has the best wear pattern and a smoothly increasing rate of flank wear. On the other hand, the performance of CBN

cutting tool with composition 3 is not as good. The total cutting length of CBN 3 is less than 30,000 m, and it has the steepest tool wear pattern compared to other CBN cutting tools. CBN cutting tool with composition 2 shows the longest tool life (104,620 meter of cutting length), almost double the length of CBN 1 and thrice that of CBN 3. It was observed that CBN 1 has the most adhesion material on rake face compared to other CBN cutting tools, which may be the reason that the change of cutting tool geometry after a certain length of flank wear causes a dramatically increasing rate of built-up layer formation on the rake face and eventual loss of tool life compared to CBN 2.

CBN 1 has the greatest % content of CBN particles, but second longest tool life out of four of the chosen CBN cutting tools. It may cause a greater tendency of boron from the workpiece material to diffuse into ferrite [70], [71].

Chapter 5: Effect of Cutting Speed on CBN Tool Wear Behavior

5.1. Experimental Procedure

Based on the last experiment, the tool wear behavior of four types of CBN cutting tools were identified. Selecting the CBN cutting tool with the best wear resistance, the following cutting conditions were used to study the effect of cutting speed on CBN tool wear behavior.

Cutting Speed:	250 m/min and 800 m/min
Feed Rate:	0.125 mm/rev
Depth of Cut:	0.3 mm on radius
Cutting Fluid:	Flood coolant, semi-synthetic, 8-10% concentration
Tool Failure Criteria:	2400 m of total cutting length

Two parallel machinability tests were conducted using a low cutting speed (250 m/min) and high cutting speed (800 m/min). The same workpiece material was used to ensure consistent GCI microstructure and mechanical properties. The three orthogonal force components: radial force, feed force and cutting force were measured with the dynamometer as shown in Figure 3.3-2. The forces were compared with the cutting length under two cutting speeds (250 m/min and 800 m/min). Equation 4.6 calculates the total cutting length. After the total cutting length reaches 2400 m, the length of flank wear was measured for both the low and high cutting speed.

5.2. Results and Discussion

Based on the previous section, CBN 1 has a better tool life before the cutting length reaches 50,000 m. Therefore, this insert was selected in testing the effect of the cutting speed on tool wear behavior under a low cutting speed (250 m/min) and a high cutting speed (800m/min). The remaining cutting conditions are the same as in previous tests, and the experiment stops whenever the total cutting length reaches 2,400 m.

Three orthogonal force components were measured with a dynamometer during the cutting processes with two cutting speeds (250 m/min and 800 m/min). The following figures show the results of force measurement and flank wear measurement.

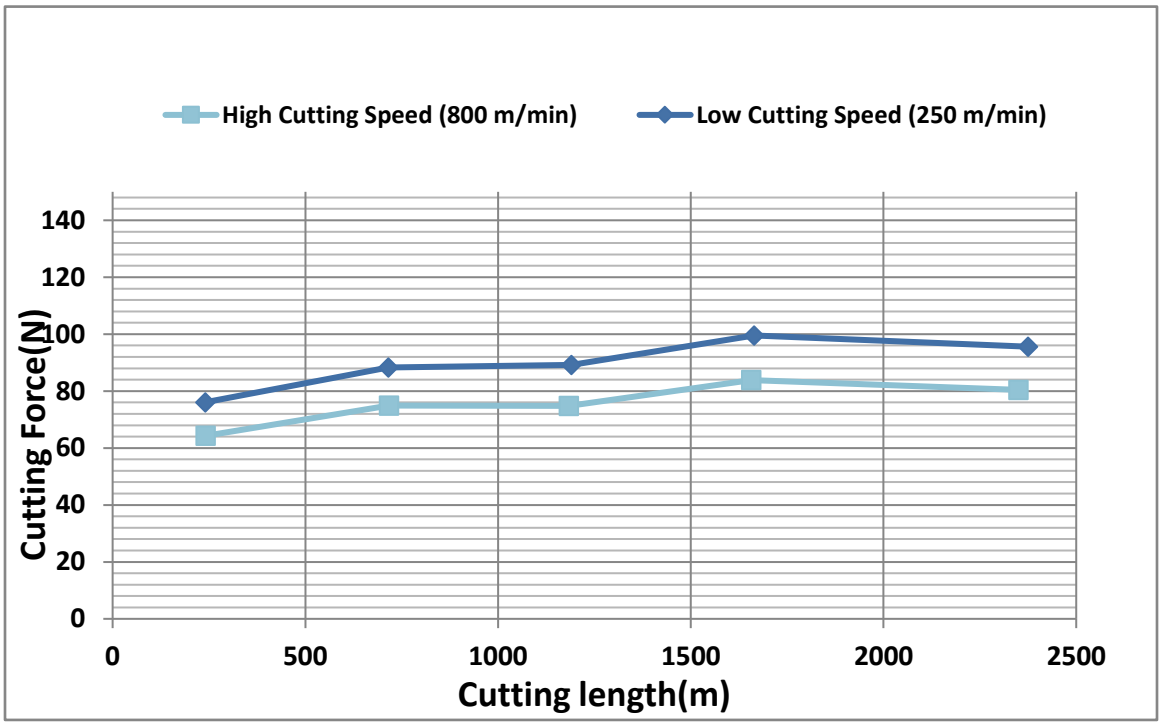

Figure 5.2-1 Relation between cutting force and cutting length.

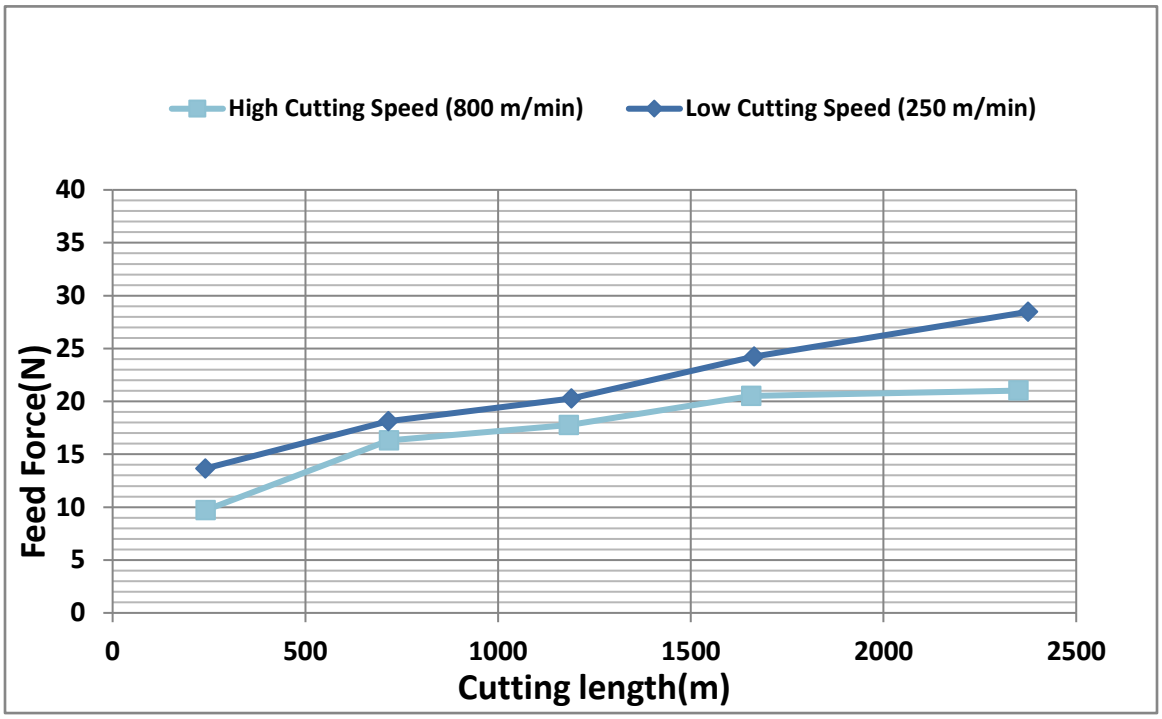

Figure 5.2-2 Relation between feed force and cutting length.

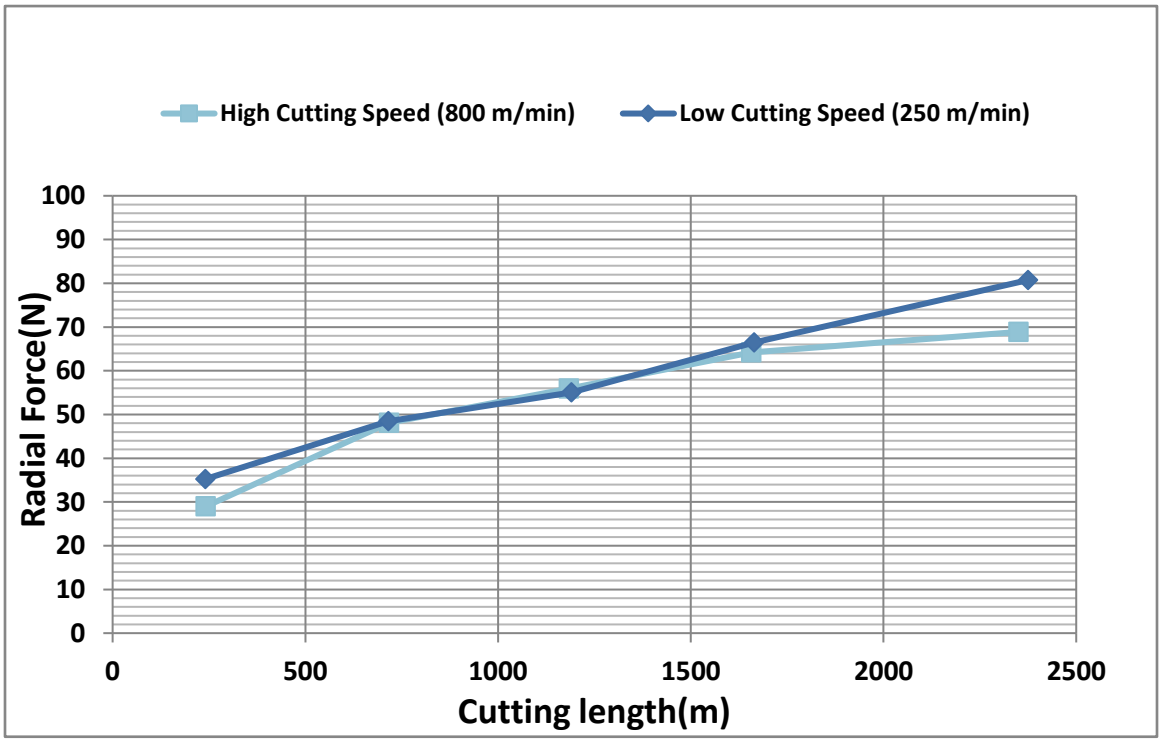

Figure 5.2-3 Relation between radial force and cutting length.

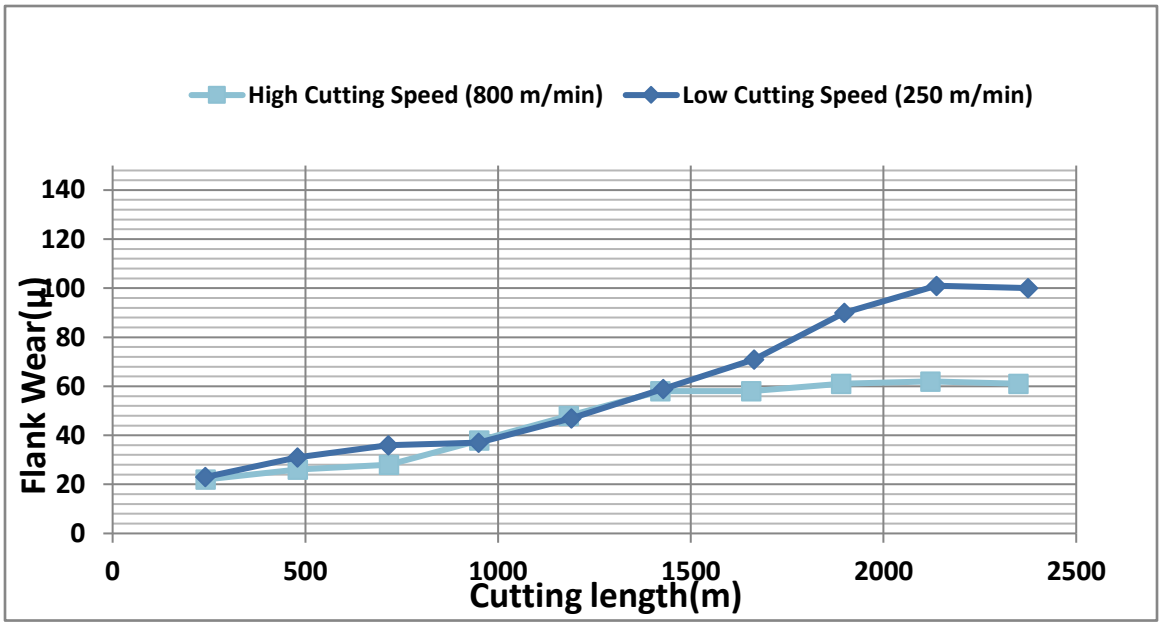

Figure 5.2-4 Relation between flank wear behavior and cutting length.

It is observed that under orthogonal cutting conditions with a high cutting speed (800 m/min) and a low cutting speed (250 m/min), CBN 1 presents less force measurements. This confirms that the high-speed machining of GCI extends the CBN tool life compared to the conventional cutting speed. The high cutting speed shows a stable and reduced rate of flank wear.

Optical microscopic images show that the lower cutting speed not only has larger flank wear but also more aggressive crater wear on tool rake face. This may be due to the longer tool-chip contact time generating more heat on tool-chip interface zone. SEM images on the tool rake face under both a low cutting speed and a high cutting speed further prove that the CBN insert with the low cutting speed has greater abrasion on the tool rake face.

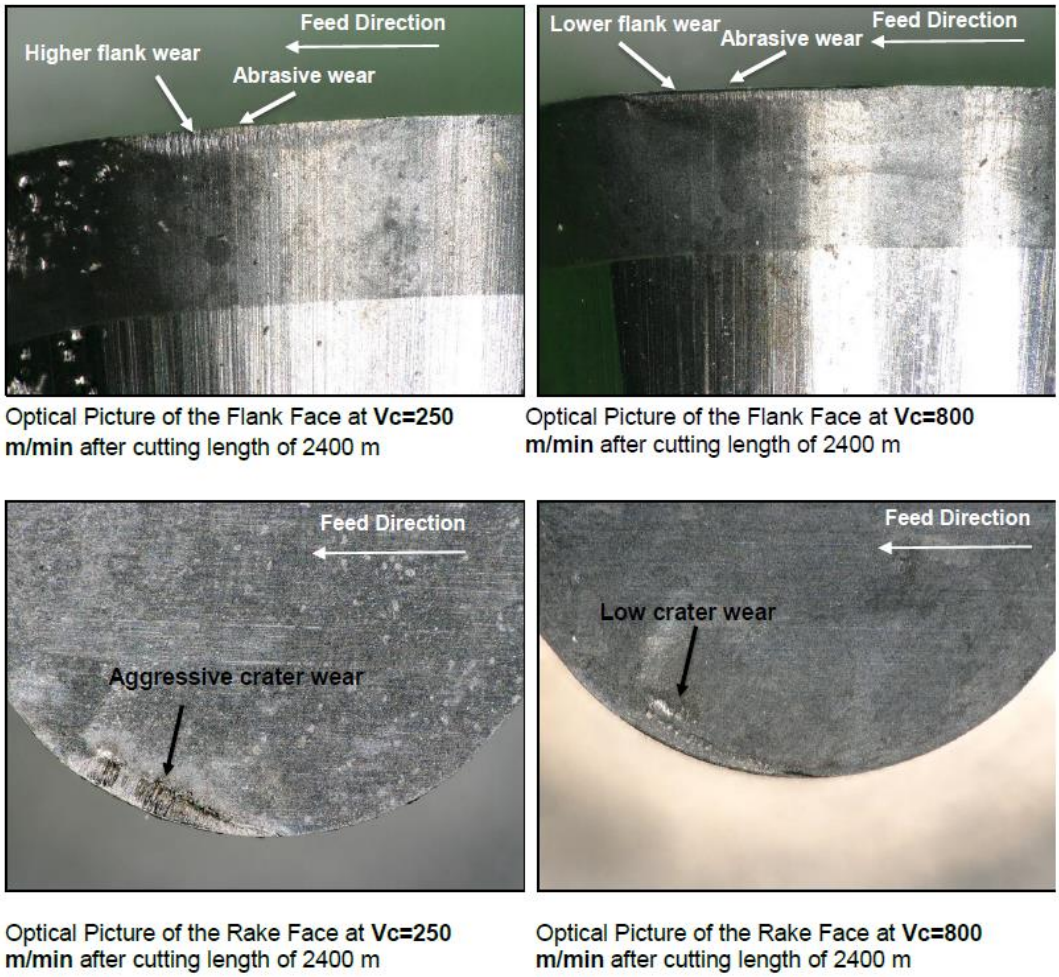

Figure 5.2-5 Optical Microscopic images of CBN inserts compostion 1 tool wear behavior with a low cutting speed (250 m/min) and a high cutting speed (800 m/min).

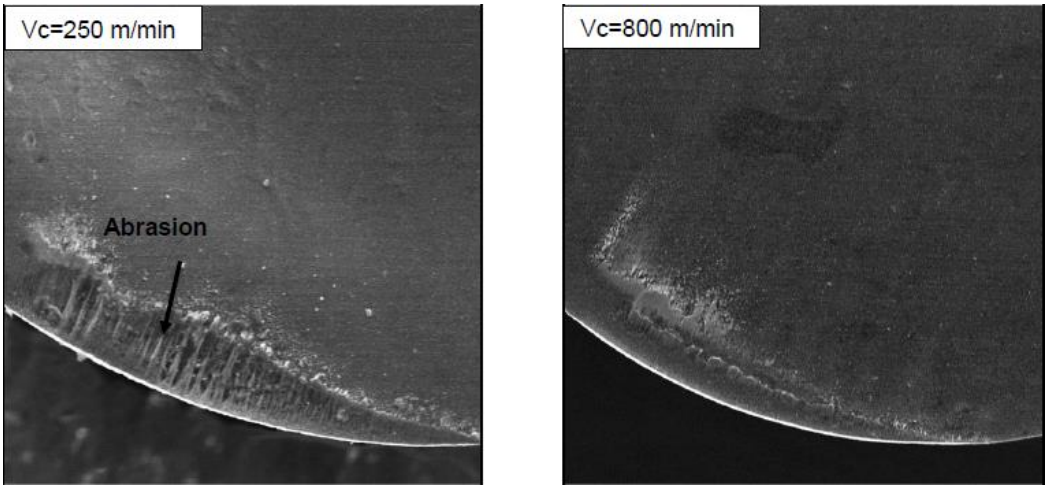

Figure 5.2-6 SEM images of tool rake face. Left one is low cutting speed, right one is high cutting speed. More abrasion wear appears on low cutting speed CBN rake face.

It has been confirmed that a high cutting speed on the GCI cylinder sleeves is likely not sacrificing tool life but in fact contributes to a better tool life. Following the results from this section, the subsequent studies keep using CBN insert composition 1.

Chapter 6: Effect of Free Ferrite Content

6.1. Experimental Procedure

Quantitative image analysis (QIA) was performed on more than 50 GCI cylinder sleeves and a table of 15 GCI sleeves with five different ranges of free ferrite content were selected for the machinability test to study the effect of free ferrite content on CBN tool wear behavior.

Table 6.1: Five ranges of free ferrite content which three GCI sleeves per range.

	Five Ranges of Free Ferrite Content				
No. Sleeves	**0 – 2.0 (%)**	**2.0 – 2.5 (%)**	**2.5 – 3.0 (%)**	**3.0 – 5.0 (%)**	**5.0 – 10.0 (%)**
1	1.44	2.29	2.74	3.99	8.63
2	1.24	2.41	2.73	3.24	5.54
3	1.31	2.47	2.74	3.11	6.76

Publications about CBN machined ferritic cast irons point out that the amount of ferrite content can significantly increase the CBN tool wear. Steadite and pearlite are iron phosphide eutectics. Both of them have a higher hardness compared to ferrite and will contribute to increased tooling abrasion wear when present. However, the effect of steadite and pearlite on tool wear is reduced in CBN tools, since typical abrasive wear is minimized due to the very high hardness of CBN. On the other hand, the quantity of free ferrite in GCI has a significant impact on machinability, particularly in CBN tools. Free ferrite is ductile and will deform significantly more than other GCI phases, increasing the required energy, cutting force and temperature on the cutting tool, which leads to accelerated chemical wear.

CBN tooling is also thought to have a direct chemical interaction with ferrite that results in rapid chemical wear (diffusion) of CBN grains and/or binder when high levels of ferrite are present in the cast iron, though the mechanisms of this wear type are only partially understood. For these reasons, it is generally recommended to keep free

ferrite to low levels (<2-5%) and to ensure suitable aging time for grey cast iron parts prior to machining.

Five levels of free ferrite were chosen based on a significant amount of QIA prior to machinability tests, using a fresh composition 1 CBN insert per level of free ferrite. A total of five fresh inserts were used in this part of the study and the cutting conditions are as follows:

Cutting Speed:	1176 m/min
Feed Rate:	0.125 mm/rev
Depth of Cut:	0.3 mm on radius
Cutting Fluid:	Flood coolant, semi-synthetic, 8-10% concentration
Tool Failure Criteria:	3000 m of total cutting length by three-cylinder sleeves

6.2. Results and Discussion

Each cylinder sleeve can be machined until a maximum cutting length of 1,000 m. Therefore, multiple sleeves are required to test one insert's wear behavior. Also, the free ferrite content for each sleeve is different to the others and a range of 5% of free ferrite content was decided for the GCI sleeves after QIA.

Free ferrite ranges from 0 – 2.0%, 2.0 – 2.5%, and 2.5 – 3.0%, were chosen to represent the conventional high-speed machining of low free ferrite content GCI workpiece. Free ferrite ranges from 3.0 – 5.0% and 5.0 – 10.0% were chosen to represent the high-speed machining of a high level of free ferrite content GCI workpiece. After cutting length reaches 3,000 m (three sleeves been machined), the tool life graph relating to % free ferrite content is shown in Figure 6.2-1.

With the increase of free ferrite content, the CBN flank wear grows linearly, while the maximum cutting length remains constant for all the testing CBN inserts, i.e. 3,000 m.

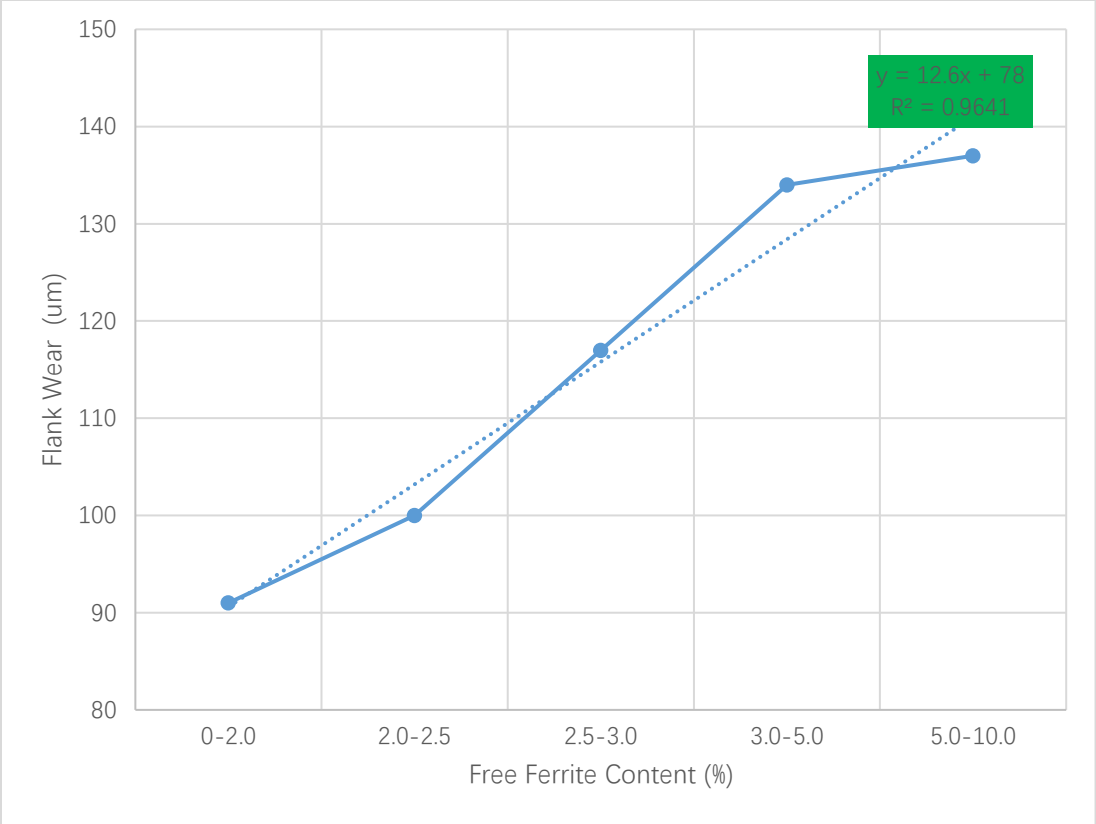

Figure 6.2-1 Effect of percent free ferrite content on CBN flank wear behavior with 3,000 m cutting length.

The rate of flank wear generation increases when the free ferrite content exceeds 2.0 % and becomes relatively stable after reaching 5.0 %. While same cutting length was set for all five fresh CBN inserts, workpiece materials with an increased range of free ferrite content possess a greater flank wear length. Compared with the first range of free ferrite content, the second range has 10 % longer flank wear, the third range 28 % greater flank wear, the fourth and fifth 47 % and 50 % greater flank wear respectively. It becomes very obvious that a greater content of free ferrite has a significant negative impact on CBN tool life and as a result, free ferrite content should not exceed 2.0 %.

SEM results with EDS mapping on the CBN tool tip, which was the CBN insert used for cutting the workpiece with first range of free ferrite (0 – 2.0 %) shows clear ferrous built-up on both tool rank and flank face. Massive ferrite adhesion on the cutting edge could cause more localized heat generation on the tool tip which reduces the CBN tool life, see Figure 6.2-2.

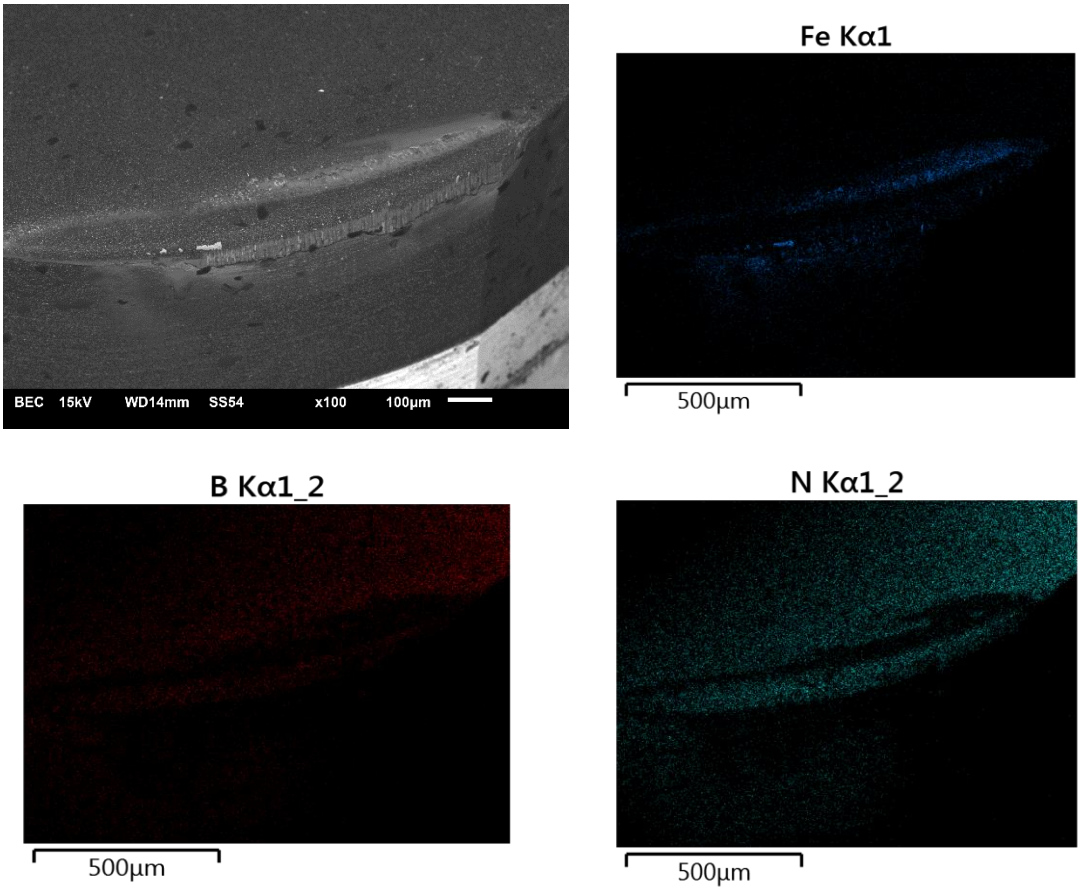

Figure 6.2-2 EDS mapping on CBN tool tip after cutting GCI workpiece with free ferrite content between 0 – 2.0 %.

Chapter 7: Influence of GCI Age Strengthening on Machinability

7.1. Experimental Procedure

To support the GCI aging study, a special lot of approximately 1200 fresh (unaged) GCI cylinder sleeves were prepared by the industrial partner on October 25th, 2017. These sleeves were shipped to the MMRI lab to be used in a full room temperature aging study, commencing on October 27th, 2017. All of the samples were stacked under room temperature. The industrial machining processes were mimicked in MMRI lab by a Boehringer VDF 180 CM CNC turning center using the following industrial cutting conditions.

Cutting Speed:	1176 m/min
Feed Rate:	0.125 mm/rev
Depth of Cut:	0.3 mm on radius
Cutting Fluid:	Flood coolant, semi-synthetic, 8-10% concentration
Tool Failure Criteria:	300 µm length of flank wear

Since QIA takes a long time to produce workpiece microstructure results, it was skipped while the artificial room temperature GCI age strengthening was in progress.

Every two days, sleeves were machined until a fresh CBN tool was fully worn; producing a set of experiments relating tool life to age of the sleeves. In parallel to machinability testing, a material characterization study was initiated to track how the hardness of the GCI cylinder sleeve material changed with aging progression. Previously published research shows that the GCI aging phenomena is the precipitation of stable iron nitride (Fe4N) into soft ferrite. Observing how the hardness of GCI cylinder sleeves changes over time would provide additional data to support machinability testing results.

7.2. Results and Discussion

7.2.1. Machinability Test

Prior to the beginning of the aging study, the experimental set-up had been used extensively in related tests including identifying optimal CBN grades and the cutting speed. These tests were completed using “fully aged” sleeves with free ferrite content fewer than 2%. The preliminary tests validate the set-up prior to the beginning of the aging test, establishing a benchmark tool life in the range of 20,000 m – 100,000 m of cut. The aging study was completed with this same set-up, identical in all aspects except for the sleeves being cut.

The result of the aging study is shown in Figure 7.2-1. Initial tests demonstrated tool life of approximately 1000 m, which improved over the first 5 days to 2500 m. The expectation was that tool life would continue to increase and eventually reach the same life as previous tests on fully-aged liners, being somewhere in the range of 20,000 m – 100,000 m of cut. Day 7.5 showed a significant drop of tool life and was the first sign that testing was not proceeding as expected, based on fully aged GCI preliminary tests. Given this unexpected result, testing was repeated on day 8.5, showing the highest life of the experiment after approximately 3700 m of cut, but still far short of the 100,000 m of tool life achieved in the previous tests on fully aged cylinder sleeves.

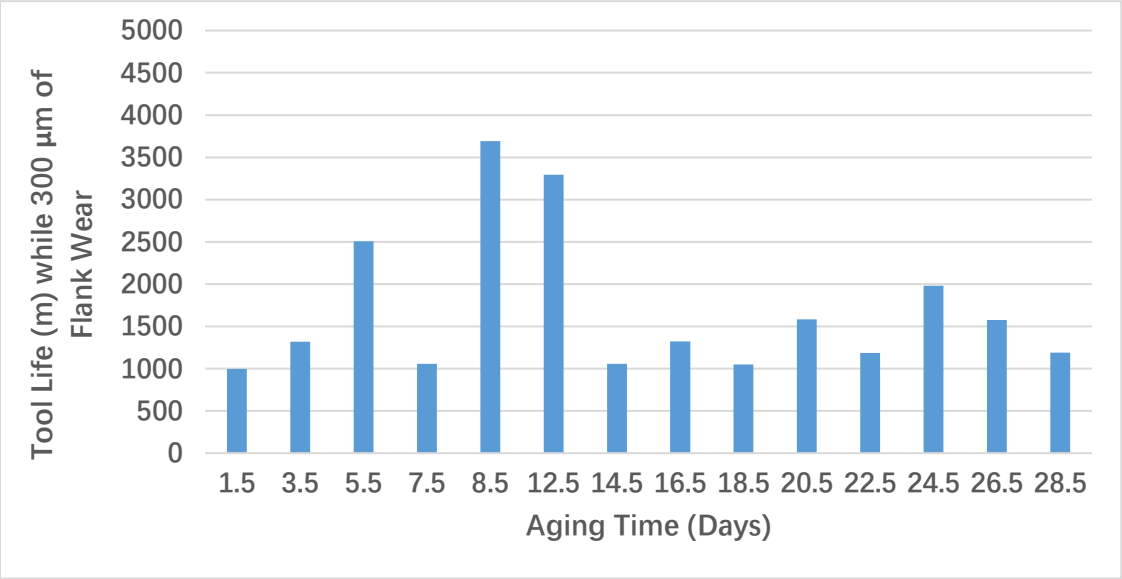

Figure 7.2-1 Variating tool life as room temperature aging processing. Very poor machinability at all stages of testing.

After day 8.5, tests continued to show very poor life, well below what was expected from previous trials. The first assumption was that this was due to a problem with the experimental set-up. Extensive measures were undertaken to determine why the tool life was lower than in the previous tests:

- Quadruple-check of all equipment, set-up, tooling, and test procedures
  - No set-up tooling, equipment or procedural issues identified
- Repetitions of past experiments to ensure results matched
  - All repetitions of past studies agreed with past results

After considerable effort, no issues with the set-up or experiment were found that could explain the lower tool life. All repetitions of previous tests, (fully aged sleeves) agreed with past results. One such test is shown as Figure 7.2-2. All aspects of the two tests shown are identical, except for material – one was completed with "fully aged" sleeves collected from industrial partner's production between June 2017 – August 2017, and the other was completed with sleeves taken from the special aging batch produced on October 25, 2017.

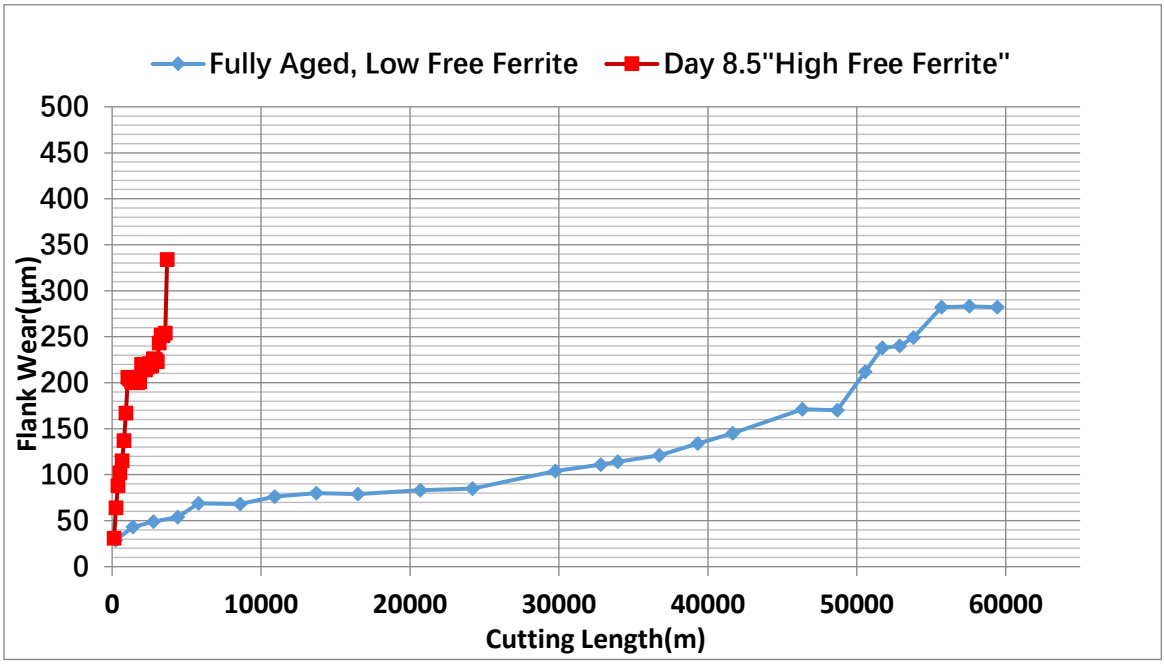

Figure 7.2-2 Tool life test results comparing fully aged sleeve with low free ferrite and sleeve from aging study with high free ferrite.

In summary, the aging study did not produce expected results; while low tool life was initially expected on the unaged fresh sleeves, tool life was considerably lower at all points during the test compared to preliminary test results on fully aged sleeves collected from the industrial partner's production between June 2017 – August 2017.

After significant effort to eliminate other possible explanations, the material composition was confidently identified as the only possible source of the unexpectedly low tool life.

7.2.2. Metallographic Inspection

As the study progressed, metallographic inspection of the samples from the Oct. 25th batch showed that approximately half of the sleeves inspected had a very high "free" ferrite content (more than 10% of free ferrite) as shown in Figure 7.2-3. High levels of free ferrite are known to significantly affect tool life in high speed machining with CBN tools. While the precise mechanism is still being understood and currently being the subject of intense study within MMRI, it is known that free ferrite interacts chemically with CBN

grains and/or binder, causing significantly accelerated tool wear, particularly at high cutting speeds where additional heat is available to drive chemical wear. The results from Chapter 6: also proves that the incremental percent content of free ferrite significantly accelerates the tool wear formation. Therefore, CBN tools are generally not recommended for machining high-ferrite containing materials.

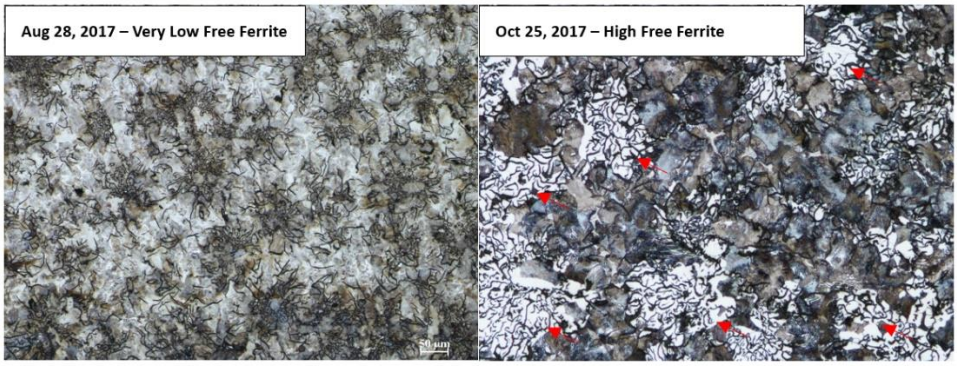

Figure 7.2-3 Comparison of free ferrite content in a "normal" sleeve and a sleeve from the Oct 25th production run.

7.2.3. Hardness Testing

In parallel to machinability testing, a material characterization study was initiated to track how the hardness of the GCI cylinder sleeve changed with time, starting from Oct 27, 2017. Von L. Richards and Wayne Nicola [23] mention an hardness increase of about 3% - 15% could be expected once GCI had fully aged. Observing how the hardness of GCI cylinder sleeves changed over time would provide additional data to support machinability testing results. Unfortunately, the machinability tests were unsuccessful due to the material issues described above, and therefore it was not possible to observe hardness evolution. However, the results are included here for posterity.

The test showed an approximately 15% increase in nano-hardness after 30 days, agreeing well with theory, see Figure 7.2-4. A spike in hardness was seen on days 23 and 25 which indicates that machinability may change significantly on these days.

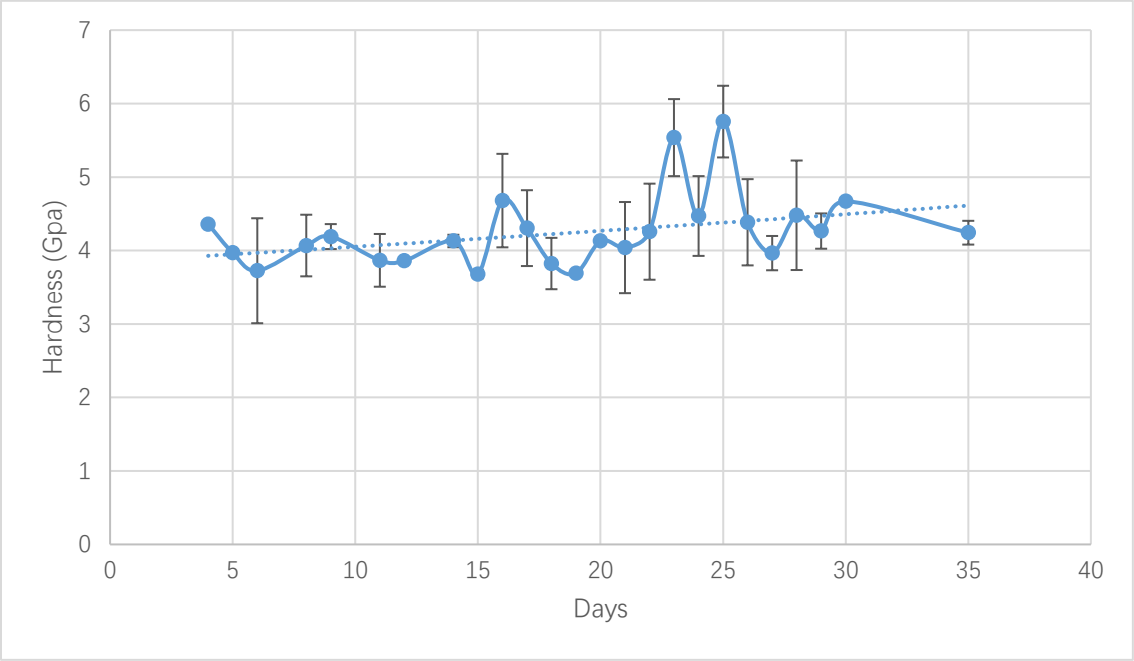

Figure 7.2-4 Results of hardness progressing with time as measured by nano-indentation

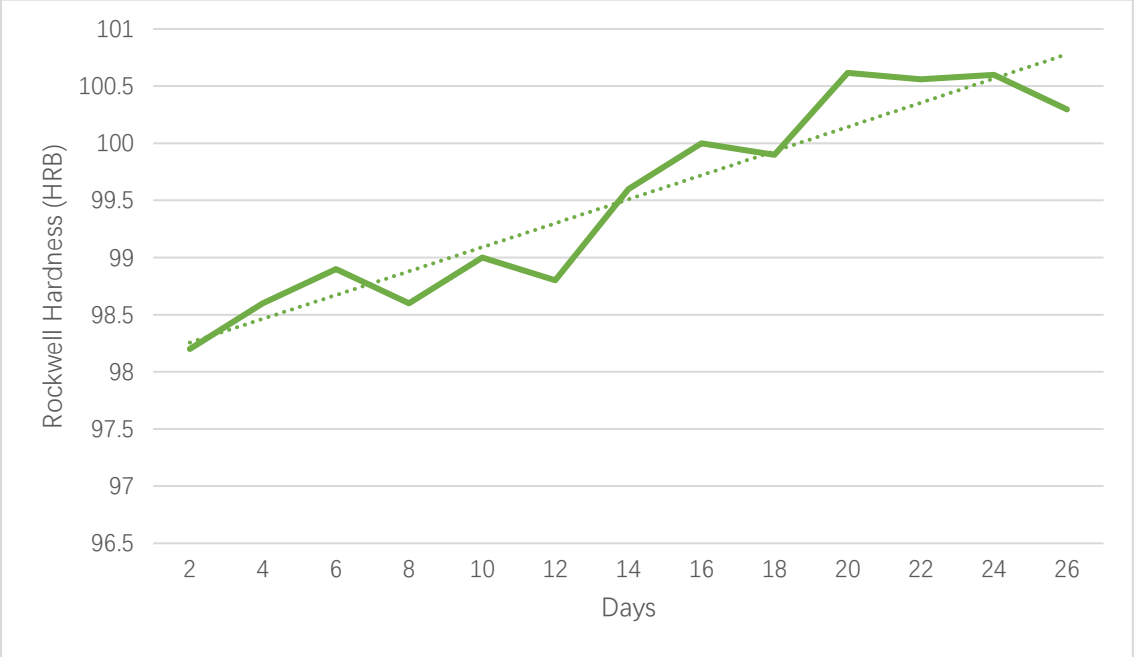

Figure 7.2-5 Results of hardness progressing with time as measured by Rockwell Hardness indentation.

In addition, after 30 days room temperature aging, the Rockwell-hardness tests show a macro -hardness increase of about 2%, which demonstrates that GCI room temperature aging contributes to the volume of hardness. Since iron nitride precipitates

into ferrite, the nano-indentation was directly on the ferrite phase, the results of which are more obvious than in the Rockwell hardness measurements.

Chapter 8: Seasonal Effect

8.1. Experimental Procedure

Though the relationship between seasons and difficult-to-machine sleeves seemed to be that of poor machinability corresponding to the colder months, only one year of data was available to support this, see Figure 1.3-1. And so, it was not reasonable to expect that the issue would arise again. Therefore, a long-term material study of incoming GCI cylinder sleeves from the industrial partner was initiated:

- Collect 2 sleeves per week from industrial partner
- Extract samples from each sleeve and prepare for metallurgical analysis
- Perform inspection to measure material properties:
    - Vickers' microhardness (HV)
    - Graphite measured via Quantitative Image Analysis (QIA)
        - Graphite flake size and percentage of area
- Attempt to relate material properties to tool life as reported by industrial partner (the best measure of machinability)

This effort progressed for approximately 14 months, beginning in late 2015 and ending in early 2017. Frustratingly, despite spanning two winter seasons, the issues with the industrial partner's difficult-to-machine sleeves did not surface during this study – the machinability of the sleeves within the industrial process remained relatively stable.

8.2. Results and Discussion

In an attempt to understand the root cause driving seasonal "difficult-to-machine" sleeves, see Figure 1.3-1 from Introduction. Sleeves were collected from the industrial partner's weekly production and subjected to material characterization to quantify graphite size and shape as well as hardness - the material properties most relevant to machinability. Graphite size, shape and area % were quantified using

quantitative image analysis (QIA) since graphite contrasts well against an un-etched microstructure. A standard Vickers microhardness indenter was used to measure hardness.

Extensive measures were undertaken to accurately and repeatedly quantify free ferrite area %, since it was also known to be a factor in the machinability of grey cast iron. With one sleeve inspected every 2 weeks, 6 samples taken from each sleeve, and 5 inspection locations per sample, nearly 800 ferrite measurements would need to be completed and thus a more practical method was needed to provide accurate and repeatable results. The following techniques were explored, but none were able to reliably and practically quantify with suitable accuracy:

- Scanning Electron Microscope using Energy-Dispersive X-Ray Spectroscopy (EDS)
- X-ray Diffraction Spectroscopy (XRD)
- Quantitative Image Analysis (QIA); extensive efforts in sample preparation and etching technique to preferentially color free ferrite

The challenge in quantifying “free” ferrite was largely due to the low amounts of it present in the GCI cylinder samples in the initial study, leading the MMRI to believe that a method capable of +/- 1% area was needed to properly quantify the free ferrite in relation to machinability. As a suitable method could not be found, the assessment of free ferrite on a weekly basis was not practical and was excluded from this study. However, its role in machinability was not forgotten and was eventually carried out by a visual estimate of free ferrite based on etched metallographic images (QIA).

If difficult-to-machine sleeves are indeed linked to seasons, a relationship would be expected to become apparent between the ambient temperature and a certain property of the material. During a period of study starting in 2015 and ending early 2017, the seasonal study results reflected no significant trends seen between hardness, graphite or ambient temperature, see Figure 8.2-1 and Figure 8.2-2. This leads to the

initial assumption that the variation of machinability is not influenced by the seasonal ambient temperature.

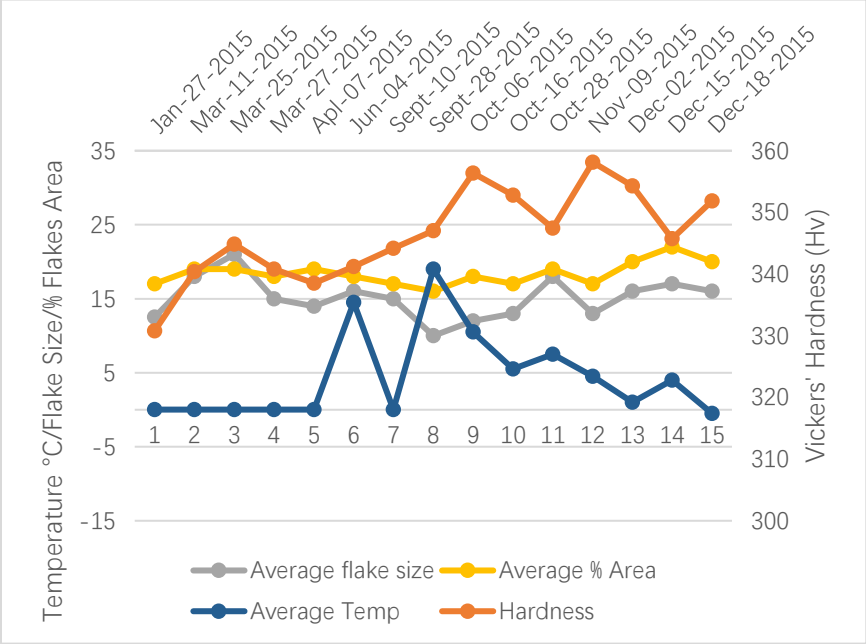

Figure 8.2-1 GCI sleeves' mechanical properties in 2015.

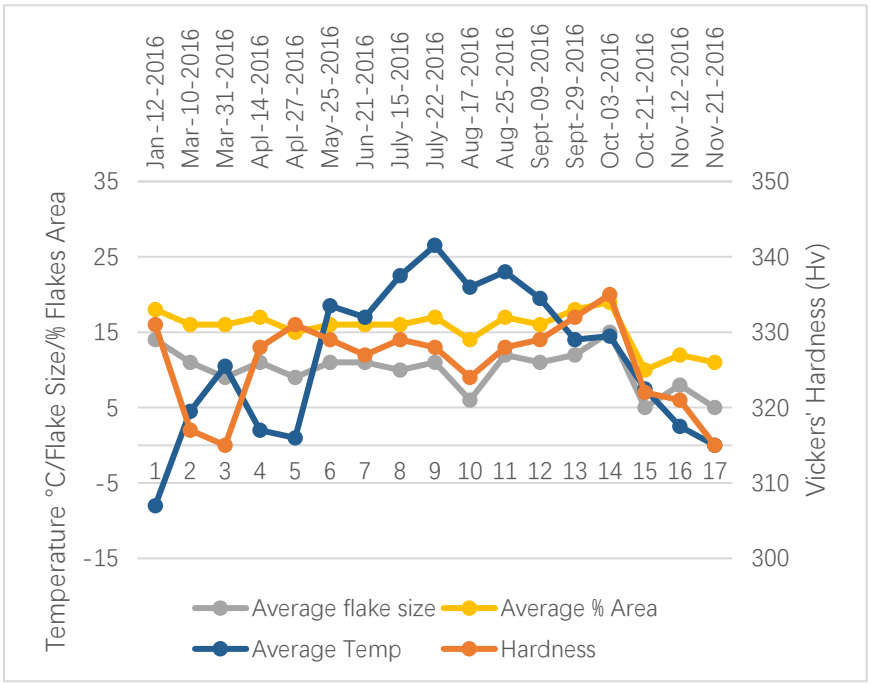

Figure 8.2-2 GCI sleeves' mechanical properties in 2016.

Chapter 9: Conclusions and Future Work

9.1. Conclusions

With support from an industrial partner, this research's purpose is to solve the seasonal variation of GCI machinability using four study directions. First, the preliminary machinability tests determine the selection of optimal CBN inserts and cutting conditions. Later on, a study is conducted of the impact of free ferrite content on CBN tool wear behavior. The next study focuses on the improvement of GCI machinability through room temperature artificial aging. Lastly, the studies of the seasonal variation of machinability, the effect of free ferrite and room temperature aging, were combined.

The CBN cutting tool with composition 1has the second longest tool life (around 50,000 m cutting length). To ensure consistency with the industrial partner and to simulate their practical conditions in the MMRI lab, it was selected as the cutting tool for running all the experimental tests. The tests confirmed that the high-speed cutting process resulted in the improvement of CBN tool life.

The % content of free ferrite has a significant influence on CBN tool wear behavior, especially under high speed machining. The soft ferrite requires more energy to plastically deform and generates more heat during the chip removal process. The additional heat and built-up ferrite layer create a greater tendency of crater and flank wear. Usually, the CBN tool life is limited by abrasion on the flank face by its own hard CBN particles, but a greater content of free ferrite in the workpiece material also leads to boron diffusion and crater wear on the rake face. The CBN tool life is much lower under high free ferrite content GCI machining.

The room temperature aging study did not produce the expected results. The tool life during the one-month aging period was inconsistent, but still considerably low. It was confirmed by QIA that this batch of GCI cylinder sleeves contained a much higher level of free ferrite. More than half of the workpiece inspected, had over 10% of free

ferrite content. The hardness results showed that the progression of room temperature aging of fresh GCI cylinder sleeves increases the hardness and consequently, the tool life. Once aging is finished, the high level of free ferrite content negates the effect of hardness increase, which explains the variation of consistently poor machinability during the one-month aging period.

The study of the two years period of seasonal effect arrives at no strong result. However, the combination of all the results obtained from this research point to the inconsistency of free ferrite content of workpiece material as being the primary cause for the seasonal variation of machinability. A final QIA inspection traced back to the difficult-to-machine sleeves during 2017, shows strong evidence that workpiece material containing low free ferrite possesses excellent machinability, but high or moderate free ferrite poor one, see Figure 9.1-1. Somehow in the beginning, the inconsistent machinability was attributed to seasonal ambient temperature and rate of aging changes followed by an ambient temperature change.

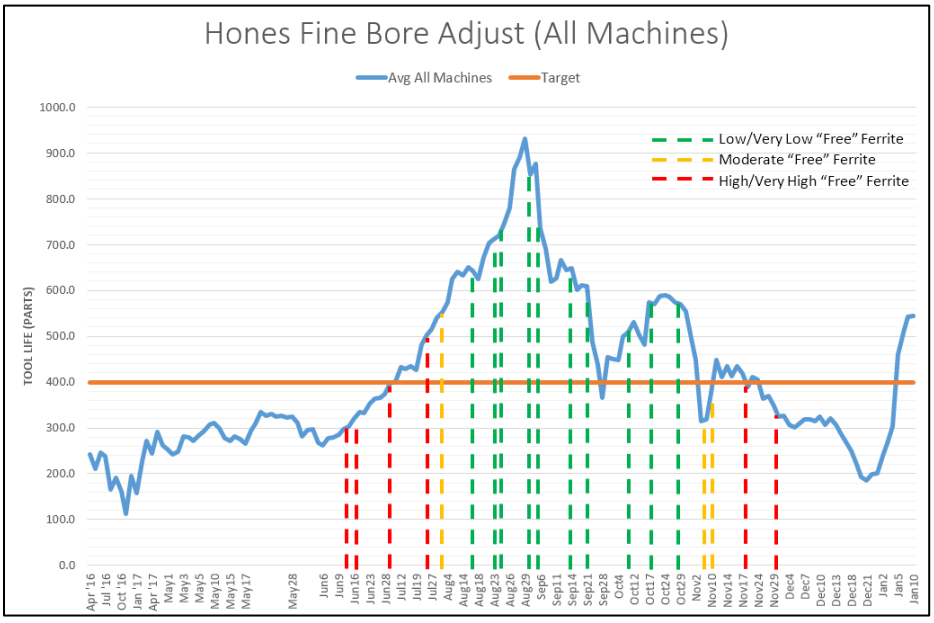

Figure 9.1-1 Tool life changes with variation of free ferrite content.

9.2. Future Work

1. Since free ferrite can cause accelerating of CBN tool wear, the phenomena is still unclear, not much literature cover this topic. Discovering wear mechanism between CBN and free ferrite is important. Why it is free ferrite not pearlite, since pearlite is a combination of ferrite and cementite. Dose free ferrite chemically react with CBN particles or the binder material and lead to a diffusion wear.
2. Study the reason causing the inconstancy of free ferrite content of GCI cylinder sleeves over times (seasonal variation).
3. Sometime, it cannot to avoid machine high free ferrite content GCI workpiece. Since CBN is not working well in this situation what kind of cutting tool can replace CBN inserts and improve the machinability while aging is still working.

Reference

[1] G. F. Vander Voort, *Metallography: Principles and practice*, vol. 18, no. 3. 1985.

[2] J. Liu, K. Yamazaki, H. Ueda, N. Narutaki, and Y. Yamane, "Machinability of Pearlitic Cast Iron With Cubic Boron Nitride (CBN) Cutting Tools," *J. Manuf. Sci. Eng.*, vol. 124, no. 4, p. 820, 2002.

[3] M. Mizutani, "Super High-speed Face Milling By CBN Cutting Tool," *Tool Eng.*, pp. 49–53, 1996.

[4] E. Trent and P. K. Wright, *Metal Cutting*. 2000.

[5] J.R. Davis, "Classification and Basic Metallurgy of Cast Irons," in *ASM Specialty Handbook Cast Irons*, 1996.

[6] H. K. Toenshoff and B. Denkena, "Chip formation," *Basic Cut. Abras. Process.*, pp. 21–37, 2013.

[7] G. E. Kempka, "Embrittlement, Toughening, and Subcritical Thermal Treatment of Malleable Iron," *AFS Trans.*, 1955.

[8] W. M. Nicola and V. Richards, "Age Strengthening of Gray Cast Iron , Phase I : Statistical Verification," *AFS Trans.*, 1999.

[9] D. M. Stefanescu, "Solidification and modeling of cast iron - A short history of the defining moments," *Mater. Sci. Eng. A*, vol. 413–414, pp. 322–333, 2005.

[10] ASM, *Metals Handbook*. 1998.

[11] M. Schmidt and K. Rohrbach, "ASM Handbook, Volume 1: Properties and Selection: Irons, Steels, and High-Performance Alloys," *Met. Handb.*, vol. 1, no. February 1990, pp. 793–800, 1990.

[12] S. Genculu, "Cast Irons --Properties and Applications."

[13] K. S. Rao, "ANALYSIS OF ENGINE CYLINDER LINERS," *Int. Res. J. Eng. Technol.*, 2015.

[14] I. Standard, "ISO 185, Grey cast irons- Classification." 2005.

[15] I. Revised, A. Gray, I. Castings, and T. S. A. E. Standard, "Vehicle," 2000.

[16] "Standard Specification for Gray Iron Castings," in *ASTM/A48*, vol. 03, no. Reapproved 2008, 2008,

pp. 1–5.

[17] L. Collini, G. Nicoletto, and R. Konečná, “Microstructure and mechanical properties of pearlitic gray cast iron,” *Mater. Sci. Eng. A*, vol. 488, no. 1–2, pp. 529–539, 2008.

[18] P. Fiorini and G. Byrne, “The influence of built-up layer formation on cutting performance of GG25 grey cast iron,” *CIRP Ann. - Manuf. Technol.*, vol. 65, no. 1, pp. 93–96, 2016.

[19] A. A. Pereira, L. Boehs, and W. L. Guesser, “The influence of sulfur on the machinability of gray cast iron FC25,” *J. Mater. Process. Technol.*, vol. 179, no. 1–3, pp. 165–171, 2006.

[20] I. Standard, “ISO 945-1, Microstructure of cast irons.” 2008.

[21] P. Vincenzo and E. Fiorini, “High Efficiency Cutting of GG25 Grey Cast Iron by,” 2015.

[22] R. Ebner, “Giesserei,” vol. 50, pp. 689–691, 1963.

[23] V. Richards and W. Nicola, “FINAL TECHNICAL REPORT : AGE STRENGTHENING OF GRAY CAST IRON PHASE III,” 2003.

[24] T. V. Anish, “Age strengthening of gray cast iron : alloying effects and kinetics study,” 2007.

[25] V. Richards, T. Anish, S. Lekakh, D. Van Aken, and W. Nicola, “Age strengthening of gray iron - Kinetics study,” *International Journal of Metalcasting*. 2008.

[26] V. L. Richards, D. C. Van Aken, and W. Nicola, “Age strengthening of gray cast iron,” *Int. J. Cast Met. Res.*, vol. 16, no. 1–3, pp. 275–280, 2003.

[27] Jared Ashley teague, “Dependency of machinability in gray cast iron on nitride-induced age strengthening,” 2010.

[28] T. Anish, S. N. Lekakh, and V. L. Richards, “The Effect of Ti and N on Iron Age Strengthening,” *AFS Trans.*, 2008.

[29] P. V. Novichkov, “Novichkov, P.V., "Thermocyclic Aging of Cast Iron at 200 - 280 Degrees C," Liteinoe Proizvodstvo (in Russian), 31-5 (1970).,” *Liteinoe Proizv. Russ.*, no. 31–5, 1970.

[30] V. L. Richards and W. Nicola, “Age strengthening of gray cast iron phase III,” *AFS Trans.*, vol. Report

Num, no. 749–55, pp. 1–9, 2003.

[31] J. Edington, W. Nicola, and V. L. Richards, “Age Strengthening of Gray Cast Iron : Nitrogen Effects and Machinability,” *AFS Trans.*, 2002.

[32] P. B. Burgess, “Age Hardening Ferritic Malleable,” *AFS Trans.*, no. 172–9, 1969.

[33] G. R. Booker, A. L. Sutton, and D. Phil, “An Investigation of Nitride rPrecipitates in Pure Iron and Mild Steels,” *J. Iron Steel Inst.*, no. 205–15, 1957.

[34] I. Fall and J. M. R. Genin, “Mössbauer spectroscopy study of the aging and tempering of high nitrogen quenched Fe-N alloys: Kinetics of formation of Fe16N2nitride by interstitial ordering in martensite,” *Metall. Mater. Trans. A Phys. Metall. Mater. Sci.*, 1996.

[35] L. J. Dijkstra, “Precipitation Phenomena in the Solid Solutions of Nitrogen and Carbon in Alpha Iron below the Eutectoid Temperature,” *Trans. Metall. Soc. AIME*, vol. 185, pp. 252–260, 1949.

[36] U. Dahmen, P. Ferguson, and K. H. Westmacott, “A TEM Study of α’’-Fe16N2 and γ’-Fe4N Precipitation in Iron-Nitrogen,” *Acta Metall.*, vol. 35, no. 5, 1987.

[37] J. F. Enrietto, “Solubility and Precipitation Of Nitrides in Alpha-Iron Containing Manganese,” *Trans. Metall. Soc. AIME*, vol. 224, no. 1, pp. 43–48, 1962.

[38] K. F. Hale and D. McLean, “Structure of Quench-Aged Iron-Carbon and Iron-Nitrogen Alloys,” *J. Iron Steel Inst. London*, vol. 201, no. 337–52, 1963.

[39] I. Hrivňák, “Low-Temperature Ageing of Iron and Low Carbon Steel,” *Met. Treat. Drop Forg.*, no. 175–81, 1961.

[40] K. H. Jack, “Binary and Ternary Interstitial Alloys. I. The Iron-Nitrogen System: The Structures of FeFormulaN and FeFormulaN,” *Proc. R. Soc. A Math. Phys. Eng. Sci.*, vol. 195, no. 1040, pp. 34–40, 1948.

[41] K. H. Jack, “The Occurrence and the Crystal Structure of Formula-Iron Nitride; a New Type of Interstitial Alloy Formed during the Tempering of Nitrogen-Martensite,” *Proc. R. Soc. A Math. Phys.*

Eng. Sci., vol. 208, no. 1093, pp. 216–224, 1951.

[42] V. A. Phillips, “An Electron Microscope Study of Quench-Aging and Strain- Aging in A Dilute Fe-C-N Alloy,” *Trans. ASM*, vol. 56, no. 600–17, 1963.

[43] D. V. Edmonds and R. W. K. Honeycombe, “Precipitation in Iron-Base Alloys,” *Met Soc. AIME Precip. Process. Solids*, 1978.

[44] S. N. Lekakh and V. L. Richards, “Aging and Machinability Interactions in Cast Iron,” *Trans. Am. Foundry Soc.*, vol. 120, no. 12-026, pp. 307–318, 2012.

[45] V. L. Richards, T. V Anish, S. Lekakh, D. C. Van Aken, and W. Nicola, “Composition Effects on Age Strengthening of Gray Iron,” *AFS Trans.*, 2006.

[46] H. Schulz, “The History of High-Speed Machining,” *Rev. Ciência e Tecnol.*, pp. 9–18, 1999.

[47] H. Schulz and T. Moriwaki, “High-speed Machining,” *CIRP Ann. - Manuf. Technol.*, vol. 41, no. 2, pp. 637–643, 1992.

[48] A. Ber and M. Goldblatt, “The Influence of Temperature Gradient on Cutting Tool’s Life,” *CIRP Ann. - Manuf. Technol.*, vol. 38/1, pp. 69–73, 1989.

[49] A. K. . C. A. B. Chattopadhyay, “Mechanism of crater wear growth of coated carbides in high speed machining,” *J. Inst. Eng. 1 ndial Prod. Eng. Div.*, vol. 70, 1989.

[50] B. P. Sarmah and M. K. Khare, “Some investigations of the wear mechanisms of widalon carbide inserts in machining EN24 (317 M 40) steel,” *Wear*, vol. 127, pp. 229–238, 1988.

[51] S. Foshag, “Neue Schneidstoffe und Beschichtungen,” *Welkstatt und Betr.*, vol. 122, no. 12, pp. 1085–1087, 1989.

[52] R. Porat, Nahariya, A. Ber, and Haifa, “New Approach of Cutting Tool Materials - CERMET (Titanium Carbonitride-Based Material) for Machining Steels,” *CIRP Ann. - Manuf. Technol.*, 1990.

[53] A. Ippolito, R., Levi. R.. Lombardi. F., Tomincasa. S.. Villa, “High speed turning: technological and economical involved aspects,” *CIRP Semin. Torino*, pp. 12–14, 1989.

[54] R. F. Silva, J. M. Gomes, A. S. Miranda, and J. M. Vieira, “Resistance of Si3N4 ceramic tools to thermal and mechanical loading in cutting of iron alloys,” *Wear*, 1991.

[55] Venkatesh. V. C., “High speed machining of cast iron and steel,” *Ann. ClRP*, vol. XV, pp. 387–391, 1967.

[56] F. Koenigsberger and J. Tlusty, *Structure of Machine Tools*. 1971.

[57] Y. Huang, Y. K. Chou, and S. Y. Liang, “CBN tool wear in hard turning: A survey on research progresses,” *Int. J. Adv. Manuf. Technol.*, vol. 35, no. 5–6, pp. 443–453, 2007.

[58] S. Takatsu, Shimoda, and Otani, “Effects of CBN content on the cutting performance of polycrystalline CBN tools,” *Int. J. Refract. Hard Met*, vol. 2, no. 4, pp. 175–178, 1983.

[59] D. A. Stephenson and J. S. Agapiou, *Metal Cutting Theory and Practice Third Edition*. 2016.

[60] V. Piispanen, “Lastunmuodostumisen teoriaa,” *Tek. Aikakausl.*, vol. 27, p. 315–322 (in Finnish), 1937.

[61] V. Piispanen, “Theory of formation of metal chips,” *J. Appl. Phys.*, vol. 19, no. 10, pp. 876–881, Oct. 1948.

[62] H. Ernst and M. E. Merchant, “Chip formation, friction and high quality machined surfaces,” *Surf. Treat. Met. ASM*, vol. 29, pp. 299–378, 1941.

[63] M. E. Merchant, “Basic Mechanics of the Metal-Cutting Process,” *J. Appl. Mech*, vol. 11, pp. 168–175, 1944.

[64] M. E. Merchant, “Mechanics of the metal cutting process. I. Orthogonal cutting and a type 2 chip,” *J. Appl. Phys.*, vol. 16, pp. 267–275, 1945.

[65] M. E. Merchant, “Mechanics of the metal cutting process. II. Plasticity conditions in orthogonal cutting,” *J. Appl. Phys.*, vol. 16, no. 6, pp. 318–324, Jun. 1945.

[66] G. Poulachon, A. Moisan, and I. S. Jawahir, “Tool-wear mechanisms in hard turning with polycrystalline cubic boron nitride tools,” *Wear*, vol. 250–251, pp. 576–586, 2001.

[67] M. Dogra, V. S. Sharma, and J. Dureja, “Effect of tool geometry variation on finish turning - A review,”

J. Eng. Sci. Technol. Rev., vol. 4, no. 1, pp. 1–13, 2011.

[68] S. OOMEN-HURST, “PROCESS OPTIMIZATION IN MACHINING: AN APPLIED RESEARCH APPROACH,” 2012.

[69] *ASM Handbook Volume 15: Casting*. 1991.

[70] SECO, *PCBN Technical Guide* -. 2009.

[71] L. N. L. de Lacalle, A. Lamikiz, J. F. de Larrinoa, and I. Azkona, “Chapter 2: Advanced Cutting Tools,” *Mach. Hard Mater.*, pp. 33–86, 2011.